Received: 31 July 2019 | Revised: 2 January 2020 | Accepted: 11 January 2020

DOI: 10.1002/eqe.3256

RESEARCH ARTICLE

WILEY

Intensity measure conversion of fragility curves

Akiko Suzuki | **Iunio Iervolino**

Dipartimento di Strutture per l'Ingegneria e l'Architettura, Università degli Studi di Napoli Federico II, Naples, Italy

Correspondence
Akiko Suzuki, Dipartimento di Strutture per l'Ingegneria e l'Architettura, Università degli Studi di Napoli Federico II, Naples, Italy.
Email: akiko.suzuki@unina.it

Funding information
European Comission, Horizon 2020 program, Grant/Award Number: 691213; Presidenza del Consiglio dei Ministri – Dipartimento della Protezione Civile, ReLUIS program

Summary

In seismic risk assessment of structures, fragility functions are the probabilistic characterization of vulnerability at the component and/or structural level, expressing the probability of *failure* as a function of a ground motion intensity measure (IM). Fragility curves, in general, are structure- and site-specific, thus a comparison of fragility curves, then of vulnerability, is not straightforward across multiple structures. Also, it could be the case that hazard at a site of interest is not available for the IM originally considered in the fragility assessment. These situations require to convert fragility curves from an original IM to a target one. The present study addresses a hazard-consistent probabilistic framework for converting spectral acceleration-based IMs from an original IM to a target IM at a given site. In particular, three conversion cases, under different assumptions on the explanatory power of the involved IMs with respect to structural failure, are discussed: (a) a vector-valued IM consisting of the original and target IMs, magnitude, and source-to-site distance; (b) a vector-valued IM consisting of the original and target IMs; and (c) the original (scalar) IM only, assuming that structural response, given the IM, is statistically independent of the other ground motion variables. In this framework, the original fragility functions are characterized using the state-of-the-art methods in performance-based earthquake engineering, then the fragility curves as a function of the target IM are evaluated through applications of the probability calculus rules, ensuring consistency with the seismic hazard at the site of interest. The conversion strategy is illustrated through the applications to three-, six-, and nine-story Italian code-conforming reinforced concrete buildings designed for a high-hazard site in Italy. The study shows that, in most of the cases, the converted fragility curves have agreement with the reference curves directly developed in terms of the target IM. Cases in which least agreement was found are likely due to the models used to obtain the terms required by the conversion equations.

KEYWORDS

performance-based earthquake engineering, probabilistic seismic risk assessment, seismic vulnerability, vector-valued intensity measures

1 | INTRODUCTION

Probabilistic seismic risk assessment of structures evaluates the rate of earthquakes capable of causing structural failure. As an application of the total probability theorem, the *failure rate* is obtained by integrating seismic fragility and seismic hazard, both expressed in terms of the same ground motion (GM) intensity measure (IM) serving as a link between the two probabilistic models. The choice of the IM to be employed in the risk analysis is mainly determined by some desired properties, eg., *sufficiency*, *efficiency*,[1] and *scaling robustness,*[2] besides *hazard computability*,[3] which is always necessary. A sufficient IM is defined as one that yields structural response, given IM, statistically independent of earthquake magnitude and source-to-site distance, while an efficient IM is defined as one that provides a comparatively low conditional *record-to-record variability* of structural response. With respect to scaling robustness, it is desirable to employ an IM which leads to unbiased structural response under scaled GM records compared with the results from as-recorded GMs. Hazard computability refers to the possibility of deriving a hazard curve in terms of that IM.

IMs for fragility assessment have been extensively investigated in research. Time-domain peak GM characteristics, such as peak ground acceleration (PGA), are classic IMs still widely used in practice because developed seismic hazard models are typically expressed in terms of these IMs. Currently, elastic spectral acceleration at the first mode vibration period of the structure, $Sa(T)$, is the most common IM. This is supported by studies which claim that it is usually more efficient than PGA and sufficient in several practical cases.[4] Nonetheless, other studies have discussed that $Sa(T)$ can be neither efficient nor sufficient in specific situations.[1,5] Advances with respect to $Sa(T)$ include vector-valued IMs or, in general, spectral-shape-based IMs.[6-10] Some other studies also explored IMs based on nonlinear structural response of simple systems,[2] yet the usage of those advanced IMs, both scalar and vector-valued, is still not widespread in practice.

Particularly in seismic risk assessment for a portfolio of multiple structures, it is needed to opt for an IM (or a set of IMs), which meets the desired IM properties for each structure. Although a seismic reliability comparison should be made in terms of annual failure rate computed with structure-specific IMs, it could be still needed to translate fragilities into a target IM, for example, in one of the following situations: (a) hazard is available only in terms of a particular IM (eg, PGA[11]) or desirable to be expressed with a single IM which is different from the IM originally used for the fragility of an individual structure (eg, for a large portfolio of heterogenous buildings across a region);[12,13] (b) it is needed to compare relative seismic vulnerability among structures excluding the hazard effects from the comparison;[14-16] and (c) it is expected to reassess fragilities after performing structural response analyses with a given IM (eg, in system analysis of large infrastructures conventionally using PGA).[17,18] To address these issues, some studies discuss the IM conversion of fragility curves. For example, Ohtori and Hirata[19] explored the IM conversion from spectral velocity at the first mode vibration period of a structure to PGA based on the *first-order second-moment* approximation,[20] although the relationship between original and target IMs is not fully characterized with respect to site's hazard. Michel et al[14] convert fragility curves between spectral accelerations at different periods, yet consistency of the proposed approach with the rules of probability calculus is not clear.

Extending preliminary research on the subject,[21] the study presented herein addresses a probabilistic framework for converting spectral acceleration-based IMs of seismic fragility curves. In particular, possible conversion cases under different assumptions on the explanatory power of the concerned IMs are explored. The fragility curve of a structure in terms of the target intensity (IM_2) is obtained through hazard-consistent conversion of a fragility function derived from structural response given the original intensity (IM_1). The probabilistic framework considers three different cases about the IMs involved: (a) a vector-valued IM consisting of IM_1, IM_2, magnitude (M), and source-to-site distance (R), that is, $\{IM_1,IM_2,M,R\}$; (b) a vector-valued IM consisting of IM_1 and IM_2, that is, $\{IM_1, IM_2\}$; and (c) the original IM_1, which is supposed to be a sufficient IM, not only with respect to M and R, but also with respect to IM_2.

The IM conversion is performed using the equivalent single-degree-of-freedom (ESDoF) systems for multiple-story Italian code-conforming reinforced concrete (RC) buildings. All the original fragility functions are obtained with the state-of-the-art methods for structural response analysis within the *Performance-Based Earthquake Engineering* (PBEE) framework:[22] eg, the *multiple-stripe analysis* (MSA) method,[23] with *hazard-consistent* record selection based on the *conditional spectra*[24] (CS). For the sake of hazard computability, the original IM herein is the spectral acceleration at a period close to the fundamental period of the corresponding structure, and the structural response data are used to perform the IM conversion when IM_2 is (a) PGA or (b) the spectral acceleration at a period larger than that of the original IM. For comparison, a *reference* fragility curve expressed in terms of IM_2 is also evaluated performing nonlinear dynamic analyses (NLDAs) using records selected directly considering IM_2 as the (original in this case) IM.

The remainder of the paper is structured such that the next section introduces the framework for converting fragility curves, followed by the models for estimating seismic fragility adopted in the study. In particular, regression models, involving the original and target IMs and magnitude and distance metrics, are used for the original fragility assessment. The next section describes the examined IM conversions including the structural models and seismic hazard under consideration. The results of the original fragility assessment of the examined structures, and site-specific seismic hazard terms, are then discussed. Subsequently, reference fragilities, whose parameters are estimated via a maximum likelihood estimation approach, are described. Finally, the results of the converted fragility curves for all IM conversion conditions/cases are addressed. Notable remarks conclude the study.

2 | METHODOLOGY

This section introduces the probabilistic framework for converting IMs of seismic fragility curves. In what follows, it is assumed that structural fragility, in terms of the original IM_1, is obtained through NLDA and that the analyst aims at converting the fragility in terms of the target IM_2 without further structural response analyses. The IM conversion involves probabilistic modelling of conditional seismic hazard and fragility, through which the fragility in terms of the target IM_2 is evaluated. In particular, this study addresses the conversion between spectral-acceleration-based IMs, considering three conversion cases under different assumptions on the variables involved. The following provides the conversion equations as well as the products from probabilistic seismic hazard analysis (PSHA) required in the conversion.

2.1 | Conversion equation

Assuming that the probability of *failure* (denoted as F) conditional to the joint occurrence of IM_1 and IM_2, $P[F|\, IM_1 = x \cap IM_2 = y]$, is available for a structure assumed to be located at a site of interest, the probability of failure given a certain (y) value of IM_2, that is $P[F|\, IM_2 = y]$, can be computed as per Equation (1) based on the total probability theorem as follows:

$$P[F|IM_2 = y] = \int_{IM_1} P[F|IM_1 = x \cap IM_2 = y] \cdot f_{IM_1|IM_2}(x|y) \cdot dx, \tag{1}$$

where $f_{IM_1|IM_2}$ is the conditional probability density function (PDF) of IM_1 given IM_2, in one earthquake of unspecified other characteristics.

The term $P[F|\, IM_1 = x \cap IM_2 = y]$ is a fragility surface evaluated through structural analysis, while $f_{IM_1|IM_2}$ is computed via the tools of PSHA.[25,26] Because PSHA typically considers earthquake magnitude and source-to-site distance as random variables (RVs), Equation (1) should be further extended to Equation (2) as follows:

$$\begin{aligned} P[F|IM_2 = y] &= \int_{IM_1} \iint_{MR} P[F|IM_1 = x \cap IM_2 = y \cap M = w \cap R = z] \cdot f_{IM_1,M,R|IM_2}(x,w,z\,|\,y) \cdot dz \cdot dw \cdot dx \\ &= \int_{IM_1} \iint_{MR} P[F|IM_1 = x \cap IM_2 = y \cap M = w \cap R = z] \cdot f_{IM_1|M,R,IM_2}(x\,|\,w,z,y) \cdot f_{M,R|IM_2}(w,z\,|\,y) \cdot dz \cdot dw \cdot dx. \end{aligned} \tag{2}$$

In the equation, $P[F|\, IM_1 = x \cap IM_2 = y \cap M = w \cap R = z]$ is the failure probability conditional to the joint occurrence of $\{IM_1, IM_2, M, R\}$; $f_{IM_1,M,R|IM_2}$ is a site-specific function that can be seen as the product of two PDFs: $f_{IM_1|M,R,IM_2}$ and $f_{M,R|IM_2}$. As discussed in the following, the former can be obtained from a GM prediction equation (GMPE) considering the statistical dependency between IM_1 and IM_2 conditional to M and R, that is, via *conditional hazard*,[26] which is factually equivalent to *vector-valued* PSHA.[27] The latter is computed through seismic hazard *disaggregation*[28] that provides the probability (density) of a certain M and R scenario given the occurrence of $IM_2 = y$. Equation (2) yields the failure probability conditional only to the target IM by marginalizing out the other three variables

from the fragility function. It can be considered the framing equation as it involves all the basic RVs entering the conversion problem.

2.2 | Conversion using a vector-valued IM consisting of IM_1 and IM_2

If the hypothesis that the vector-valued IM, $\{IM_1, IM_2\}$, is sufficient cannot be rejected, then structural response given the IM can be considered, by definition, statistically independent of M and R. This means that these variables have negligible influence in predicting the structural response, ie, $P[F|\, IM_1 = x \cap IM_2 = y \cap M = w \cap R = z] = P[F|\, IM_1 = x \cap IM_2 = y]$. Hence, Equation (2) reduces to

$$P[F|IM_2 = y] = \int_{IM_1} P[F|IM_1 = x \cap IM_2 = y] \cdot \iint_{MR} f_{IM_1|M,R,IM_2}(x \mid w,z,y) \cdot f_{M,R|IM_2}(w,z \mid y) \cdot dz \cdot dw \cdot dx, \tag{3}$$

which is identical to Equation (1). This conversion equation, considering a two-parameter-vector-valued fragility function, is useful in case additional consideration of IM_2 helps to improve efficiency in structural response assessment, as discussed in the studies endorsing the use of vector-valued IMs for seismic risk assessment of structures.

2.3 | Conversion using a single intensity measure: IM_1

If the original IM_1 is a sufficient IM not only with respect to magnitude and distance but also with respect to IM_2, Equation (3) can be further simplified as per Equation (4) as follows:

$$P[F|IM_2 = y] = \int_{IM_1} P[F|IM_1 = x] \cdot \iint_{MR} f_{IM_1|M,R,IM_2}(x \mid w,z,y) \cdot f_{M,R|IM_2}(w,z \mid y) \cdot dz \cdot dw \cdot dx. \tag{4}$$

In the equation, $P[F|IM_1 = x]$ is the original fragility curve of the structure. Note that the case of nonsufficient IMs, in principle, can be addressed by hazard-consistent record selection, such that the simplified equations presented in this section can still be applied.

The multi- or single-variable fragility functions in Equations (2) to (4) can be derived via a numerical approach, which one can choose from a variety of methods for assessing probabilistic seismic fragility. For the sake of generality of the conversion framework, the fragility evaluation models considered particularly in this study will be separately introduced in Section 3.

2.4 | Hazard conversion terms

This subsection describes the procedures to characterize the terms that depend on the probabilistic seismic hazard of the site in the IM conversion equations, Equations (2) to (4), that is, the probability distributions conditional to the target IM_2, $f_{IM_1|M,R,IM_2}$ and $f_{M,R|IM_2}$, corresponding to the second and third integrands, respectively.

The calculations to obtain the PDFs of IM_1 conditional to IM_2 and a specific magnitude-distance scenario, $f_{IM_1|M,R,IM_2}$, have been discussed in previous research.[6,26] Given that GMPEs exist for the two IMs, the following equations hold:

$$\begin{cases} \ln IM_1 = \mu_{\ln IM_1|M,R} + \sigma_{\ln IM_1} \cdot \varepsilon_{\ln IM_1} \\ \ln IM_2 = \mu_{\ln IM_2|M,R} + \sigma_{\ln IM_2} \cdot \varepsilon_{\ln IM_2} \end{cases}, \tag{5}$$

where $\mu_{\ln IM_1|M,R}$ $\left[\mu_{\ln IM_2|M,R}\right]$ is the mean of the logarithm of IM_1 $[IM_2]$ conditional to a certain magnitude-distance scenario $\{M,R\}$, $\sigma_{\ln IM_1}$ $[\sigma_{\ln IM_2}]$ is the standard deviation of the logarithm of IM_1 $[IM_2]$, and $\varepsilon_{\ln IM_1}$ $[\varepsilon_{\ln IM_2}]$ is a standard normal variable, also known as *standardized residual*. Equation (5) typically allows to assume that the two IMs are (marginally) lognormally distributed conditional to $\{M,R\}$.

Under the assumptions that the logarithms of the two IMs, conditional to magnitude and source-to-site distance, are jointly-normal, then the conditional distribution $f_{IM_1|M,R,IM_2}$ is the PDF of a lognormal RV. Conditional to the target IM_2, magnitude, and distance, the parameters of the Gaussian distribution associated to $f_{IM_1|M,R,IM_2}$ are

$$\begin{cases} \mu_{\ln IM_1|\ln IM_2,M,R}(y,w,z) = \mu_{\ln IM_1|M,R}(w,z) + \rho_{\ln IM_1,\ln IM_2}\cdot\sigma_{\ln IM_1}\cdot\dfrac{\ln y - \mu_{\ln IM_2|M,R}(w,z)}{\sigma_{\ln IM_2}} \\ \sigma_{\ln IM_1|\ln IM_2} = \sigma_{\ln IM_1}\cdot\sqrt{1-\rho^2_{\ln IM_1,\ln IM_2}} \end{cases}, \tag{6}$$

where $\mu_{\ln IM_1|\ln IM_2,M,R}$ is the mean value of $\ln IM_1$ given the joint occurrence of $\{IM_2 = y, M = w, R = z\}$. The correlation coefficient $\rho_{\ln IM_1,\ln IM_2}$ can be obtained, for example, from literature studying the correlation between spectral acceleration values at different periods.[29] The other term depending on the hazard, namely, the conditional distribution $f_{M,R|IM_2}$, can be computed via hazard disaggregation.

3 | FRAGILITY ASSESSMENT

The fragility functions in the integrals on the right-hand sides of Equations (2) to (4) can be obtained through NLDA using a numerical model of the structure and a set of GM records. There is a variety of structural analysis methods to obtain the relationship between a specific IM and a structural response measure, ie, an *engineering demand parameter* (EDP). Common approaches in earthquake engineering research are *cloud analysis*,[30] *incremental dynamic analysis* (IDA),[31] and MSA. The cloud method requires performing dynamic analysis using a set of unscaled GM records collected so as to cover wide ranges of the concerned IMs. IDA collects EDP values under a single set of GM records incrementally scaled up to a certain IM value. The MSA method also involves dynamic analyses at multiple IM levels, yet it employs different record sets selected consistently to the hazard disaggregation results for each IM level (*stripe*), ie, it is hazard-consistent record selection. Among those, (unscaled) cloud analysis and MSA methods can be used to model the fragility term in Equation (2), which can be further simplified either to Equations (3) or (4) depending on the explanatory power of the selected IM. IDA using scaled records can be also an option. However, the sufficiency of the IM is needed, as hazard-consistency is generally not warranted at all IM levels using a single set of GMs, which IDA usually entails. Nonetheless, converted fragilities resulting from any conversion equations, Equations (2) to (4), are site-specific because of the hazard terms therein as described in Section 2.4.

Fragility modelling strategies for various structural analysis methods have been comprehensively discussed in literature.[7,32] From a statistical inference perspective, fragility assessment approaches can be broadly classified into *parametric* and *nonparametric*, depending on whether a parametric probabilistic model is assumed to describe structural fragility. Following a parametric approach, supposing that structural failure is the exceedance of a certain performance threshold in terms of an EDP of interest (edp_f), that is, $F \equiv EDP > edp_f$, log-linear regression models can be employed to determine the relationship between the EDP and the IM. In case the considered IM is $\{IM_1, IM_2, M, R\}$, for example, the logarithm of the EDP can be given in the form of Equation (7):[6,7]

$$\ln EDP = \ln \bar{EDP} + \eta_{\ln EDP} = \beta_0 + \beta_1\cdot\ln x + \beta_2\cdot\ln y + \beta_3\cdot w + \beta_4\cdot\ln z + \eta_{\ln EDP}, \tag{7}$$

where $\ln \bar{EDP}$ is the conditional mean given the explanatory variables $\{IM_1 = x, IM_2 = y, M = w, R = z\}$, $\{\beta_0, \beta_1, \beta_2, \beta_3, \beta_4, \sigma_\eta\}$ are regression parameters, and $\eta_{\ln EDP}$ is the regression residual.

The model defined by Equation (7) is equivalent to assuming a lognormal distribution of EDP conditional to $\{IM_1, IM_2, M, R\}$, with the mean equal to $\beta_0+\beta_1\cdot\ln x+\beta_2\cdot\ln y+\beta_3\cdot w+\beta_4\cdot\ln z$ and standard deviation σ_η. Then, the probability of EDP exceeding edp_f, conditional to $\{IM_1, IM_2, M, R\}$, can be given by Equation (8), where $\Phi(\bullet)$ is the standard normal cumulative distribution function as follows:

$$P[F|IM_1 = x \cap IM_2 = y \cap M = w \cap R = z] = 1 - \Phi\left(\frac{\ln edp_f - \ln \bar{EDP}}{\sigma_\eta}\right). \tag{8}$$

It should be noted that there are some disadvantages in estimating a fragility function through linear regression as some assumptions can be inappropriate when nonlinear structural response is concerned; see Baker.[7] In case of

performing MSA, the fragility function can be modelled fitting a regression at each IM_1 stripe, which can help at least to reduce some of these problems. Although this option is not considered in this study, relevant issues will be altogether discussed later in the application.

Another issue that often arises in structural fragility analysis is that the numerical model of the structure does not yield meaningful EDP values in cases of *numerical instability* or *collapse* according to the definition of Shome and Cornell.[4] However, in such cases, one can account for the contribution from collapse cases through a *logistic regression* model in addition to the linear regression model from noncollapse (NC) cases defined by Equation (7). In particular, a binary variable, C, is set equal to 1 if the collapse of the structure is observed, and 0 otherwise (ie, NC).[6,33] In this case, the probability of collapse can be evaluated as follows:

$$P[C|IM_1 = x \cap IM_2 = y \cap M = w \cap R = z] = \frac{\exp\left(\beta_{0,\mathrm{L}} + \beta_{1,\mathrm{L}} \cdot \ln x + \beta_{2,\mathrm{L}} \cdot \ln y + \beta_{3,\mathrm{L}} \cdot w + \beta_{4,\mathrm{L}} \cdot \ln z\right)}{1 + \exp\left(\beta_{0,\mathrm{L}} + \beta_{1,\mathrm{L}} \cdot \ln x + \beta_{2,\mathrm{L}} \cdot \ln y + \beta_{3,\mathrm{L}} \cdot w + \beta_{4,\mathrm{L}} \cdot \ln z\right)}, \tag{9}$$

where $\beta_{0,\mathrm{L}}$, $\beta_{1,\mathrm{L}}$, $\beta_{2,\mathrm{L}}$, $\beta_{3,\mathrm{L}}$, and $\beta_{4,\mathrm{L}}$ are logistic regression coefficients. The probability of failure given a vector-valued IM, that is, $\{IM_1, IM_2, M, R\}$, can be then reformulated considering the contributions from both NC and collapse data through Equations (8) and (9), respectively; ie, an application of the total probability theorem as follows:

$$P[F|IM] = P[C|IM] + P\left[EDP > edp_f | NC, IM\right] \cdot (1 - P[C|IM]). \tag{10}$$

4 | INVERSTIGATED CONVERSIONS AND STRUCTURAL MODELS

4.1 | Structures, sites, conversions

IM conversions under various conditions were explored with respect to different combinations of *Sa*-based IMs and structural performance levels (PLs). To this aim, this study considered a series of multiple-story RC frame buildings designed according to the current Italian design code (*Norme Tecniche per le Costruzioni;* NTC).[34,35] The buildings under consideration were taken from those designed, modelled, and analyzed in the *Rischio Implicito Norme Tecniche per le Costruzioni* (RINTC) project,[36] which had assessed the failure risk of new buildings with a variety of structural types/configurations and seismic hazard levels of the construction sites.

Among the structures considered in the RINTC project, this study examined three-, six-, and nine-story (3st, 6st, 9st) RC moment-resisting frame (MRF) buildings featuring three different structural configurations (ie, bare-, infilled-, and *pilotis*-frames, hereafter denoted as BF, IF, and PF, respectively; Figure 1A). Seismic design of these buildings refers to the site of L'Aquila (central Italy) on the local soil condition C (according to Eurocode 8 classification).[37] The

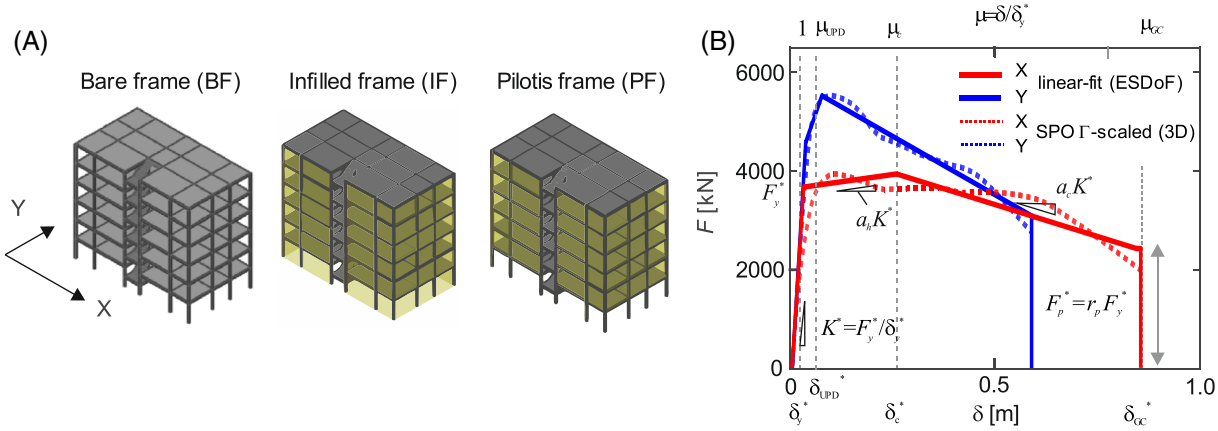

FIGURE 1 Examples of case study reinforced concrete (RC) buildings: (A) three-dimensional (3D) model and (B) static pushover (SPO) curves for the six-story [6st] pilotis-frame (PF) (after Suzuki and Iervolino)[16,21]

TABLE 1 IM conversions under consideration

PL	UPD, GC											
Stories	**3st**			**6st**			**9st**			**6st**		
Config.	**BF**	**IF**	**PF**	**BF**	**IF**	**PF**	**BF**	**IF**	**PF**	**IF**		
$IM_1 \equiv Sa(T)$	1.0 s	0.15 s	0.5 s	1.5 s	0.5 s	0.5 s	2.0 s	1.0 s	1.0 s	0.5 s	0.5 s	0.5 s
$IM_2 \equiv Sa(T)$	0 s (PGA)									1.0 s	1.5 s	2.0 s

Abbreviations: BF, bare-frame; GC, global collapse; IF, infilled-frame; IM, intensity measure; PF, *pilotis*-frame; PGA, peak ground acceleration; PL, performance level; UPD, usability-preventing damage; 3st, three-story; 6st, six-story; 9st, nine-story.

fundamental vibration periods of the considered buildings are approximately in the range between 0.3 and 2.0 seconds. For PSHA purposes, the following five periods, $T = \{0.15\text{s}, 0.5\text{s}, 1.0\text{s}, 1.5\text{s}, 2.0\text{s}\}$, were selected first, then the spectral acceleration at the closest period to the fundamental vibration periods of the structure among the five was defined as IM_1.

The IM conversions of the fragility curves were performed with respect to the exceedance of two PLs: *usability-preventing damage* (UPD) and *global collapse* (GC). Particularly, when conversions between Sa-based IMs are of concern, it is expected that whether the period of the target IM_2 is smaller or larger than that of the original IM can have an effect (see the discussion in Baker about interaction of IMs).[7] To examine the generality of the discussed approaches beyond any specific pairs of IMs, this study explored: (a) the conversion from $IM_1 \equiv Sa(T)$ to $IM_2 \equiv PGA$ for all nine buildings and (b) only for the 6st IF building whose IM_1 is $Sa(0.5\text{s})$, the conversion from $IM_1 \equiv Sa(T)$ to a spectral acceleration at each of the three discrete periods larger than 0.5 seconds, ie, $T = \{1.0\text{s}, 1.5\text{s}, 2.0\text{s}\}$. In summary, this study considered 12 conversions for each of the two PLs (Table 1).

4.2 | Structural models

The nine RC buildings under consideration are all intended for residential use. According to NTC, their seismic design refers to *damage limitation* and *life-safety* limit states corresponding to a design GM (ie, uniform-hazard spectrum)[38] with 50- and 475-year exceedance return periods (T_R), respectively. Each building is a 5 × 3 bays MRF characterized by regularity in plan and elevation, a floor area of 21.4 × 11.7m^2, and story heights of 3.05 m (except the ground floor which is 3.4 m in height). The RC frames include knee-joint beams designed to support the staircases. From a design point of view, the structural members of BF and IF are identical in dimensions and reinforcement detailing (ie, the difference lies in the presence of infills) while the vertical structural members at the ground floor of PF were strengthened to account for the infill reduction, as per the code requirements. Seismic design was performed by means of modal response spectrum analysis considering by a *behavior factor*[37] equal to 3.9. For more details on design and modelling, see Ricci et al.[36]

To reduce the computational complexity in seismic response analysis for fragility evaluation, this study utilized the ESDoF systems whose structural responses were available from previous studies.[16]* They were calibrated based on the static pushover (SPO) curve of the original three-dimensional (3D) structural models, both constructed in OpenSees.[39] The ESDoF properties, such as equivalent mass m^*, vibration period T^*, viscous damping ratio ξ^* (5%), and the characterizations of the hysteretic behavior for an idealized multi-linear backbone curve, were calculated for each structure according to Fajfar[40] in conjunction with the backbone-fitting criteria in Baltzopoulos et al.[41] Each ESDoF system features the following backbone parameters: yield strength and displacement $\left(F_y^*, \delta_y^*\right)$, post-yielding hardening and softening ratio (a_h, a_c), capping ductility $\left(\mu_c = \delta_c^*/\delta_y^*\right)$, the ratio of the residual strength to the yield strength $\left(r_p = F_p^*/F_y^*\right)$, and the failure ductility $\left(\mu_{GC} = \delta_{GC}^*/\delta_y^*\right)$.

Following the general failure criteria adopted in the RINTC project, this study defined the GC ductility so that it corresponds to 50% strength deterioration with respect to the maximum base-shear of the SPO curve for each horizontal direction. The UPD failure ductility $\left(\mu_{UPD} = \delta_{UPD}^*/\delta_y^*\right)$, considered for the IFs and PFs, was determined by the occurrence of the first among three conditions: (a) the attainment of the maximum lateral resistance in 50% of the masonry

*Note that such approximation does not affect the generality of the conversion equations.

TABLE 2 Dynamic and static pushover parameters of the ESDoF systems

Config.	Dir.	T^*, s	m^*, ton	Γ	$Sa_y(T^*)$, g	ξ^*, %	F_y^*, kN	δ_y^*, m	a_h	μ_c	a_c	r_p	μ_{UPD}	μ_{GC}
3st BF	X	0.68	534	1.30	0.51	5	2668	0.06	0.003	7.0	−0.11	0.51	0.62	11.4
	Y	0.69	543	1.29	0.49	5	2600	0.06	0.006	5.8	−0.12	0.52	0.64	10.2
3st IF	X	0.30	580	1.26	0.54	5	3059	0.01	0.07	4.6	−0.02	0.90	1.20	50.2
	Y	0.33	590	1.25	0.76	5	4422	0.02	0.04	3.1	−0.10	0.75	1.66	17.1
3st PF	X	0.47	730	1.09	0.58	5	4119	0.03	0.01	6.4	−0.03	0.61	1.31	23.5
	Y	0.50	731	1.09	0.66	5	4754	0.04	0.01	2.6	−0.04	0.60	1.21	11.8
6st BF	X	1.13	1177	1.31	0.25	5	2923	0.08	0.01	7.5	−0.15	0.54	0.88	11.0
	Y	0.87	1147	1.33	0.35	5	3941	0.07	0.02	5.1	−0.08	0.59	1.05	11.4
6st IF	X	0.57	1230	1.30	0.29	5	3485	0.02	0.03	4.7	−0.03	0.90	2.71	33.6
	Y	0.54	1247	1.30	0.43	5	5269	0.03	0.09	3.1	−0.07	0.86	1.98	17.6
6st PF	X	0.65	1401	1.26	0.27	5	3671	0.03	0.01	9.0	−0.02	0.66	2.51	30.0
	Y	0.57	1251	1.33	0.37	5	4581	0.03	0.17	2.2	−0.03	0.67	1.77	17.9
9st BF	X	1.86	1774	1.31	0.14	5	2423	0.12	0.01	7.3	−0.10	0.56	0.87	11.4
	Y	1.68	1725	1.34	0.16	5	2707	0.11	0.02	7.8	−0.08	0.68	0.91	12.9
9st IF	X	0.78	1728	1.31	0.17	5	2936	0.03	0.03	4.7	−0.02	0.85	2.64	48.8
	Y	0.84	1695	1.36	0.22	5	3589	0.04	0.12	2.6	−0.02	0.56	1.75	28.1
9st PF	X	0.87	2012	1.30	0.16	5	3140	0.03	0.02	4.2	−0.02	0.89	2.42	40.2
	Y	0.89	1853	1.33	0.21	5	3859	0.04	0.002	9.0	−0.02	0.62	1.47	28.9

Abbreviations: BF, bare-frame; ESDoF, equivalent single-degree-of-freedom; IF, infilled-frame; PF, *pilotis*-frame; 3st, three-story; 6st, six-story; 9st, nine-story.

infills, (b) the attainment of a 50% strength reduction from the maximum resistance at the member level in at least one masonry infill, and (c) the attainment of 95% of the maximum base-shear of the structure. As regards the BFs, the UPD PL was defined as the exceedance of the deformation capacity corresponding to the (roof) drift ratio of 0.5%.

As an example, Figure 1B illustrates the tri-linear backbones in the two horizontal directions for the 6st PF building (the directions X and Y indicated in Figure 1A), which lead to two uncoupled ESDoF systems for each structure (to follow). In the figure, each backbone of the ESDoF systems is compared with the SPO curve of the original 3D structural model scaled by the modal participation factor of the first-mode vibration, Γ. For the given SPO parameters of each system, a moderately pinching, peak-oriented hysteretic behavior without any cyclic stiffness/strength deterioration[42] was applied. Model parameters, including the yielding spectral acceleration at the equivalent vibration period, $Sa_y(T^*) = F_y^*/m^*$, are summarized for the considered nine RC buildings in Table 2. For more detailed information on ESDoF modelling, see Suzuki et al[43] and Suzuki.[44]

5 | ANALYSIS

Original fragilities were obtained by means of MSA performed in terms of IM_1 for the described ESDoF systems. The GM record selection and the number of stripes were defined according to the RINTC project approach. In particular, 10 $Sa(T)$ values, corresponding to the exceedance return periods $T_R = \{10,50,100,250,500,1000,2500,5000,10000,100000\}$ years, were considered according to the probabilistic seismic hazard of L'Aquila (no larger return periods were considered so as to avoid large extrapolations). The record selection was hazard-consistent by means of the CS method[24] collecting 20 GM records for each level of IM_1 (as defined in Table 1; for further details, see Iervolino et al[15]). In principle, this procedure should render the sufficiency issue of the chosen IM irrelevant; however, because of practical constraints of selection, this may not always be perfectly the case.[†] Therefore, for each structure, this study explored all three conversion equations given in Section 2.

[†]Potential hazard-inconsistency over different spectral ordinates can be improved with more advanced methods such as the modified conditional spectra (CS)–based method conditioned on average spectral acceleration (CS-aveSa[45]).

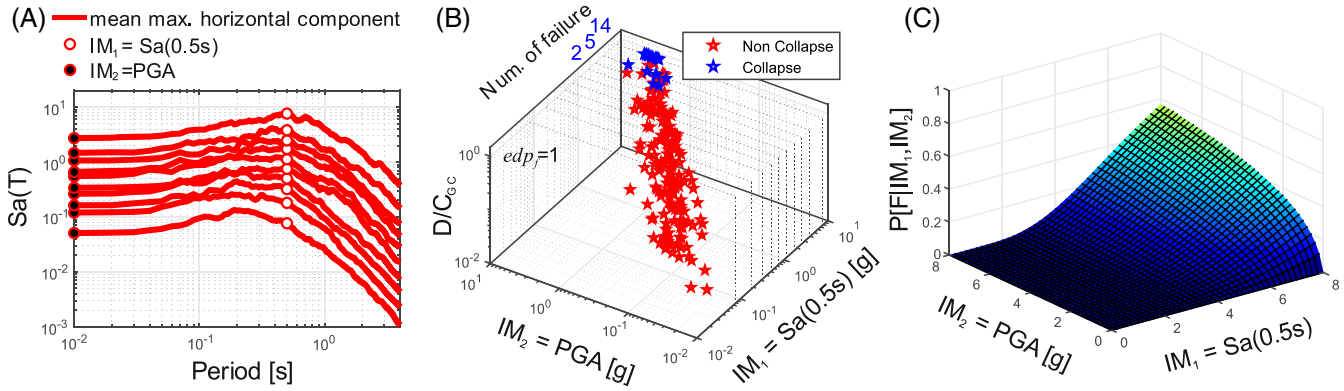

FIGURE 2 Results of original fragility assessment: (A) mean spectra of ground motion (GM) records, (B) collapse D/C ratios against the two intensity measures (IMs), and (C) collapse fragility surface using $\{IM_1, IM_2\}$

The demand-over-capacity (D/C) ratio of the displacement was considered as the EDP for both the two PLs such that $edp_f = 1$ in all cases (hereafter, the EDPs for UPD and GC are denoted as D/C_{UPD} and D/C_{GC}, respectively). Structural responses in the two horizontal directions were examined independently. This means that, in MSA, two uncoupled ESDoF systems for each structure were individually excited by two horizontal components of a GM record scaled to a certain IM level, then the larger D/C ratio of the two ESDoF systems was considered as the response. As an example, Figure 2A,B shows the mean spectra of the GM records for the ten stripes and the obtained collapse D/C ratios (D/C_{GC}) against IM_1 and IM_2 for the 6st PF building (shown in Figure 1A,B), for the case when the target IM_2 is PGA. In this case, MSA was performed up to Sa(0.5s) equal to 7.64 g, which corresponds to the largest return period of exceedance considered. For each Sa(0.5s) stripe, the response data corresponding to the failure cases are denoted with specific markers and figures, and the total number of the observations is provided in Figure 2B.

Because, even for the same structure, the assessment of the original fragility needs to be performed for each pair of $\{IM_1, IM_2\}$, the following discusses the fragility results separately for the IM conversions to PGA and for those to spectral acceleration at a larger period than that of the original IM.

5.1 | Fragility assessment for PGA as the target IM

This subsection discusses original fragilities when $IM_2 \equiv$ PGA. Multiple linear regression analyses were performed via Equation (7) using the EDP response data obtained from MSA (eg, Figure 2B). For each structure and each PL, the linear regression models involving (a) $\{IM_1,IM_2,M,R\}$, (b) $\{IM_1, IM_2\}$, and (c) IM_1 only, were obtained.[‡] In fact, these linear regression models varying the candidate variables were also used to examine the explicative power of the IMs with respect to structural response and then failure. In particular, evaluations were made based on the coefficients of the regression (related to the sufficiency of the IM) and the standard deviation of the regression residuals, σ_η (related to the efficiency of the IM).[23,33] To this aim, the regression analysis using $\{IM_1,M,R\}$ was additionally performed via Equation (7) to examine the predictive power of IM_1 for each conversion case.

Table 3 provides the regression results for the three IM cases with respect to the GC and UPD PLs, as well as those for the additional IMs. In all considered cases, the joint consideration of all four variables resulted, as expected, in the lowest σ_η values. Nonetheless, IM_1 alone generally provided σ_η values comparable with the vector-valued IMs, showing its efficiency (ie, 3st PF, 6st IF/PF, and all 9st frames). In such cases, IM_1 appeared to have a relatively large explicative power, which is supported by the regression models considering $\{IM_1,M,R\}$, that is, comparable σ_η values with those of the simple regression models using IM_1, and small regression coefficients for magnitude and distance (since the regression coefficients in the table tell changes in terms of logarithm of the EDP due to a unit change in each variable, the latter was also confirmed through standardized regressions eliminating the unit scale problem).

[‡]It should be noted that, as a possible alternative to fit the fragility functions, logistic regression analyses were also performed; however, the log-linear model setting the engineering demand parameter (EDP) values equal to 1 was found more effective to assess the global collapse (GC) fragility functions in these cases.

TABLE 3 Multiple linear regression analysis results of the original fragility assessment $IM_2 \equiv$ PGA)

	PL	UPD, $EDP = D/C_{UPD}$						GC, $EDP = D/C_{GC}$					
Config.	IM	β_0	β_1	β_2	β_3	β_4	σ_η	β_0	β_1	β_2	β_3	β_4	σ_η
3st BF	{*Sa*(1.0 s), *PGA*, *M*,*R*}	1.14	0.62	0.35	0.06	0.02	0.27	−1.63	0.66	0.34	0.05	0.01	0.27
	{*Sa*(1.0 s), *PGA*}	1.52	0.68	0.32	-	-	0.27	−1.27	0.71	0.31	-	-	0.28
	{*Sa*(1.0 s), *M*,*R*}	1.55	0.95	-	−0.02	0.01	0.33	−1.27	0.97	-	−0.02	0.004	0.32
	Sa(1.0 s)	1.42	0.93	-	-	-	0.32	−1.38	0.95	-	-	-	0.32
3st IF	{*Sa*(0.15 s), *PGA*, *M*,*R*}	0.94	−0.45	1.43	0.11	−0.0003	0.49	−2.09	−0.56	1.55	0.13	−0.03	0.51
	{*Sa*(0.15 s), *PGA*}	1.50	−0.36	1.45	-	-	0.50	−1.46	−0.44	1.57	-	-	0.52
	{*Sa*(0.15 s), *M*,*R*}	−0.24	1.04	-	0.12	−0.004	0.62	−3.32	1.07	-	0.14	−0.03	0.66
	Sa(0.15 s)	0.38	1.16	-	-	-	0.63	−2.65	1.22	-	-	-	0.67
3st PF	{*Sa*(0.5 s), *PGA*, *M*,*R*}	0.23	0.90	0.10	0.04	−0.04	0.26	−2.32	0.80	0.19	0.07	−0.09	0.33
	{*Sa*(0.5 s), *PGA*}	0.38	0.94	0.10	-	-	0.26	−2.06	0.87	0.20	-	-	0.35
	{*Sa*(0.5 s), *M*,*R*}	0.23	0.99	-	0.03	−0.05	0.26	−2.32	0.97	-	0.05	−0.10	0.34
	Sa(0.5 s)	0.31	1.02	-	-	-	0.26	−2.19	1.04	-	-	-	0.36
6st BF	{*Sa*(1.5 s), *PGA*, *M*,*R*}	1.26	0.67	0.29	0.05	0.003	0.26	−1.13	0.68	0.30	0.05	−0.007	0.27
	{*Sa*(1.5 s), *PGA*}	1.63	0.72	0.26	-	-	0.26	−0.80	0.73	0.28	-	-	0.27
	{*Sa*(1.5 s), *M*,*R*}	1.81	0.94	-	−0.02	−0.01	0.31	−0.57	0.95	-	−0.03	−0.02	0.31
	Sa(1.5 s)	1.63	0.93	-	-	-	0.31	−0.80	0.94	-	-	-	0.32
6st IF	{*Sa*(0.5 s), *PGA*, *M*,*R*}	−0.34	0.80	0.13	0.13	−0.10	0.37	−2.65	0.74	0.20	0.14	−0.11	0.40
	{*Sa*(0.5 s), *PGA*}	0.22	0.95	0.11	-	-	0.40	−2.04	0.91	0.19	-	-	0.43
	{*Sa*(0.5 s), *M*,*R*}	−0.35	0.92	-	0.12	−0.10	0.37	−2.65	0.93	-	0.12	−0.12	0.41
	Sa(0.5 s)	0.15	1.04	-	-	-	0.40	−2.16	1.07	-	-	-	0.43
6st PF	{*Sa*(0.5 s), *PGA*, *M*,*R*}	−0.37	0.74	0.17	0.15	−0.10	0.39	−2.76	0.71	0.22	0.16	−0.12	0.41
	{*Sa*(0.5 s), *PGA*}	0.25	0.91	0.14	-	-	0.42	−2.05	0.90	0.20	-	-	0.45
	{*Sa*(0.5 s), *M*,*R*}	−0.38	0.90	-	0.13	−0.11	0.40	−2.77	0.91	-	0.14	−0.13	0.42
	Sa(0.5 s)	0.16	1.03	-	-	-	0.43	−2.18	1.07	-	-	-	0.45
9st BF	{*Sa*(2.0 s), *PGA*, *M*,*R*}	1.93	0.86	0.10	0.01	0.01	0.23	−0.65	0.89	0.10	0.02	0.01	0.25
	{*Sa*(2.0 s), *PGA*}	2.05	0.87	0.10	-	-	0.23	−0.50	0.90	0.09	-	-	0.25
	{*Sa*(2.0s), *M*,*R*}	2.15	0.97	-	−0.01	0.01	0.24	−0.45	0.98	-	−0.005	0.02	0.26
	Sa(2.0 s)	2.08	0.95	-	-	-	0.24	−0.47	0.97	-	-	-	0.26
9st IF	{*Sa*(1.0 s), *PGA*, *M*,*R*}	0.56	0.78	0.17	0.10	−0.03	0.32	−2.29	0.80	0.18	0.11	−0.04	0.36

(Continues)

TABLE 3 (Continued)

Config.	PL	UPD, $EDP = D/C_{UPD}$						GC, $EDP = D/C_{GC}$					
	IM	β_0	β_1	β_2	β_3	β_4	σ_η	β_0	β_1	β_2	β_3	β_4	σ_η
	{*Sa*(1.0 s), *PGA*}	1.15	0.88	0.13	-	-	0.33	−1.62	0.91	0.13	-	-	0.37
	{*Sa*(1.0 s), *M*,*R*}	0.74	0.93	-	0.06	−0.04	0.33	−2.10	0.96	-	0.08	−0.04	0.37
	Sa(1.0 s)	1.10	0.99	-	-	-	0.33	−1.66	1.02	-	-	-	0.38
9st PF	{*Sa*(1.0 s), *PGA*, *M*,*R*}	0.46	0.80	0.09	0.12	−0.04	0.31	−2.46	0.84	0.10	0.13	−0.03	0.36
	{*Sa*(1.0 s), *PGA*}	1.16	0.93	0.04	-	-	0.32	−1.65	0.97	0.05	-	-	0.37
	{*Sa*(1.0 s), *M*,*R*}	0.56	0.88	-	0.10	−0.05	0.31	−2.35	0.93	-	0.11	−0.03	0.36
	Sa(1.0 s)	1.14	0.96	-	-	-	0.32	−1.67	1.01	-	-	-	0.37

Abbreviations: BF, bare-frame; D/C, demand-over-capacity; EDP, engineering demand parameter; GC, global collapse; IF, infilled-frame; IM, intensity measure; PF, *pilotis*-frame; PGA, peak ground acceleration; PL, performance level; UPD, usability-preventing damage; 3st, three-story; 6st, six-story; 9st, nine-story.

[Correction added on 6 March 2020 after first online publication: one missing value in Table 3 has been added in this version.]

TABLE 4 Multiple regression analysis results of the original fragility assessment ($IM_1 \equiv Sa(0.5\ s)$ and $IM_2 \equiv Sa(T > 0.5\ s)$)

	PL	UPD, D/C_{UPD}						GC, D/C_{GC}					
Config.	**IM**	β_0	β_1	β_2	β_3	β_4	σ_η	β_0	β_1	β_2	β_3	β_4	σ_η
6st IF	{*Sa*(0.5 s), *Sa*(1.0 s), *M*,*R*}	0.56	0.52	0.46	0.01	−0.05	0.29	−1.75	0.51	0.47	0.01	−0.06	0.33
	{*Sa*(0.5 s), *Sa*(1.0 s)}	0.57	0.53	0.48	-	-	0.29	−1.76	0.52	0.50	-	-	0.33
	{*Sa*(0.5 s), *Sa*(1.5 s), *M*,*R*}	1.11	0.63	0.39	−0.05	−0.05	0.30	−1.23	0.63	0.38	−0.05	−0.06	0.34
	{*Sa*(0.5 s), *Sa*(1.5 s)}	0.71	0.64	0.36	-	-	0.31	−1.61	0.64	0.36	-	-	0.35
	{*Sa*(0.5 s), *Sa*(2.0 s), *M*,*R*}	1.36	0.67	0.36	−0.06	−0.05	0.28	−1.00	0.66	0.36	−0.06	−0.06	0.33
	{*Sa*(0.5 s), *Sa*(2.0 s)}	0.87	0.67	0.33	-	-	0.29	−1.46	0.67	0.33	-	-	0.34
	Sa(0.5 s)	0.15	1.04	-	-	-	0.40	−2.16	1.07	-	-	-	0.43
	IM	$\beta_{0,L}$	$\beta_{1,L}$	$\beta_{2,L}$	$\beta_{3,L}$	$\beta_{4,L}$	R_L^2	$\beta_{0,L}$	$\beta_{1,L}$	$\beta_{2,L}$	$\beta_{3,L}$	$\beta_{4,L}$	R_L^2
	{*Sa*(0.5 s), *Sa*(1.0 s)}	-	-	-	-	-	-	−5.06	0.14	4.10	-	-	0.67
	{*Sa*(0.5 s), *Sa*(1.5 s)}	-	-	-	-	-	-	−4.33	0.82	5.21	-	-	0.72
	{*Sa*(0.5 s), *Sa*(2.0 s)}	-	-	-	-	-	-	−2.70	1.39	4.50	-	-	0.76

Abbreviations: D/C, demand-over-capacity; GC, global collapse; IF, infilled-frame; IM, intensity measure; UPD, usability-preventing damage; 6st, six-story.

However, there are a few exceptional cases. For the 3st and 6st BFs, the regression results suggest that the two-parameter model $\{IM_1, IM_2\}$ may be the best choice among the options investigated. For each structure, the two-parameter model's σ_η was comparable with that of the four-parameter regression model, while it was reduced by more than 15% with respect to the regression model using IM_1. The use of $\{IM_1, IM_2\}$ improved the performance of the model with respect to IM_1, possibly because these structures have their T^* periods relatively apart from that for $Sa(T)$ at least in one horizontal direction (see Table 2). Another exception is, as expected, the case of 3st IF: the estimates of the regression coefficients for IM_1 resulted to be negative, possibly because of the correlation of the IMs in one seismic event. The trends discussed above were observed regardless the PL considered.[§]

Based on the regression results, fragility functions were derived using Equations (7) and (8). As an example, Figure 2C illustrates the computed GC fragility surfaces using $\{IM_1, IM_2\}$ for the 6st PF building (in Figures 1 and 2A,B. It can be seen that the failure probability increases principally with IM_1 with respect to IM_2.

5.2 | Fragility assessment for spectral acceleration as the target IM

This subsection presents the results of the fragility assessment for converting the IM of fragility from $IM_1 \equiv Sa(0.5s)$ to spectral acceleration at a larger period, $IM_2 \equiv Sa(T)\ \forall\ T = \{1.0s, 1.5s, 2.0s\}$. Table 4 provides the multiple regression results of D/C_{UPD} and D/C_{GC} for these conversion cases. Generally, it is observed that $\{IM_1, IM_2\}$ reduces σ_η by approximately 20% from that estimated by the regression model considering IM_1 only. No significant change in σ_η, between the four- and two-parameter regression models, supports the conclusion on the relatively large predictive power of $\{IM_1, IM_2\}$.

It should be noted that, when IM_2 is the spectral acceleration at a period larger than the fundamental period of the structure, one challenge is to appropriately model the interaction, if any, between IM_1 and IM_2 in a linear regression. For example, as discussed in Baker,[7] structural response can be less sensitive to IM_2 at low IM_1 levels when the structure behaves in the linear range, while the sensitivity of structural response to IM_2 (or *practicality*[47] of IM_2) increases at large IM_1 levels: ie, in the nonlinear range.

As a matter of fact, the multiple linear regression results in the table show that the regression coefficients corresponding to the four explanatory variables remain almost the same between the UPD and GC performance levels and only the intercept β_0 shifts. This means that the difference in the corresponding EDP, due to one unit increase of each explanatory variable, does not change. To handle this issue, this study also attempted some alternative solutions,

[§]This study also examined the sufficiency and efficiency of the candidate intensity measures (IMs), ie, four- and two-term vector-valued IMs and the original IM, by the approach set forth by Luco and Cornell.[46] Similar results on the explanatory power of the candidate IMs as those described were observed.

TABLE 5 Correlation coefficients between IM_1 and IM_2

$\rho_{\ln IM_1, \ln IM_2}$	Sa(0.15 s)	Sa(0.5 s)	Sa(1.0 s)	Sa(1.5 s)	Sa(2.0 s)		Sa(1.0 s)	Sa(1.5 s)	Sa(2.0 s)
PGA	0.8876	0.6862	0.5243	0.4255	0.3539	**Sa(0.5 s)**	0.7490	0.6087	0.5141

Abbreviation: PGA, peak ground acceleration.

among which a logistic regression model using the collapse data was the most effective. The computed two-parameter logistic regression models using $\{IM_1, IM_2\}$ fit the observed NC and collapse data with the R-squared measure, R_L^2, given in the table.[48] Hence, the fragility surface modelled using Equations (9) and (10) was additionally examined through the conversion case using $\{IM_1, IM_2\}$ for all considered periods of IM_2.[¶] Conversely, with respect to the linear regressions, the logistic regressions showed the dominant effect of IM_2 on the EDP rather than that of IM_1 (again, confirmed through the standardized regressions eliminating the unit scale problem); see the estimates of the regression coefficients in Table 4.

As in the conversion to PGA, the original fragility functions with respect to the two PLs were principally derived via Equations (7) and (8) using the three IMs. For each different IM_2, the models combining linear and logistic regression models (defined by Equations (7)-(10); hereafter denoted as *hybrid*) were also additionally explored using $\{IM_1, IM_2\}$, in the case of GC fragility. In the linear regression models, the collapse data were included assigning the corresponding EDP values equal to 1 instead of performing the logistic regression.

5.3 | Site-specific seismic hazard functions for conversion

PSHA was performed for the site of L'Aquila in order to characterize the site-specific hazard functions required in the IM conversion framework (Section 2.4). The source model used for PSHA corresponds to *branch 921* of the logic tree involved in the official Italian hazard model.[49,50] For all target IMs, the hazard disaggregation results given IM_2 $\left(f_{M,R|IM_2}\right)$ were obtained via the REASSESS software.[51] In order to obtain a fragility function in terms of IM_2, the disaggregation was repeatedly performed at each step of IM_2 up to an upper limit value of the target IM. For all possible combinations of $\{IM_2,M,R\}$, the conditional PDF of $f_{IM_1|M,R,IM_2}$ was computed via Equation (6) using the parameters from the cited GMPEs, with the correlation model developed by Baker and Jayaram.[29] The correlation coefficients for the considered combinations of the logarithms of IMs (Table 5) show that correlation between the log of PGA and the log of the candidate $Sa(T)$ ranges between approximately 0.35 and 0.89, decreasing with an increase of the vibration period. Those between Sa(0.5s) and $Sa(T > 0.5\text{s})$ are from 0.51 to 0.75. The closer the two vibration periods, the higher the correlation coefficient for the two IMs.

To better understand this issue and its importance herein, Figure 3A shows hazard disaggregation conditional to PGA equal to 0.9 g (corresponding to $T_R = 5.6 \times 10^3$ years) at the site of interest, L'Aquila. Figure 3B,C presents the conditional distribution $f_{IM_1|M,R,IM_2}$ given PGA, magnitude $M \in (6.0,6.5)$, and $R \in (0\text{km}, 5\text{km})$, which is the scenario dominating the hazard being disaggregated in Figure 3A. It can be clearly seen from these figures that the area exhibiting a comparatively large probability density shifts from the proximity of the diagonal of the $IM_1 - IM_2$ domain (the warm-colored area in Figure 3B) to the corner corresponding to low IM_1 levels (Figure 3C) with an increase of the vibration period of IM_1 (ie, a decrease of the correlation coefficient between the logs of IM_1 and IM_2; see Table 5). Given that the original fragility functions are weighted by the corresponding hazard function through the conversion integral, it is indicated that the applicability of the adopted fragility model is important particularly in the $IM_1 - IM_2$ range showing a relatively large value of the PDF of IM_1 given IM_2.

Figure 3D,E provides similar results for one of the conversions from Sa(0.5 s) to spectral acceleration at a period larger than 0.5 seconds; ie, the hazard disaggregation conditional to $Sa(1.5\text{ s}) = 0.7$ g at the same site and the conditional distribution $f_{IM_1|M,R,IM_2}$ given Sa(1.5 s) and the dominating scenario in the disaggregation. On the contrary to Figure 3B,C, the area corresponding to the mid-to-high values of the conditional PDF widely spreads over the $IM_1 - IM_2$ domain.

[¶]In MSA for the six-story (6st) infilled-frame (IF) building, 21 collapse cases were observed in total (similar to Figure 2), thus the logistic regression on more than two predictor variables were not performed in this study (following *10-events-per-variable* rule).

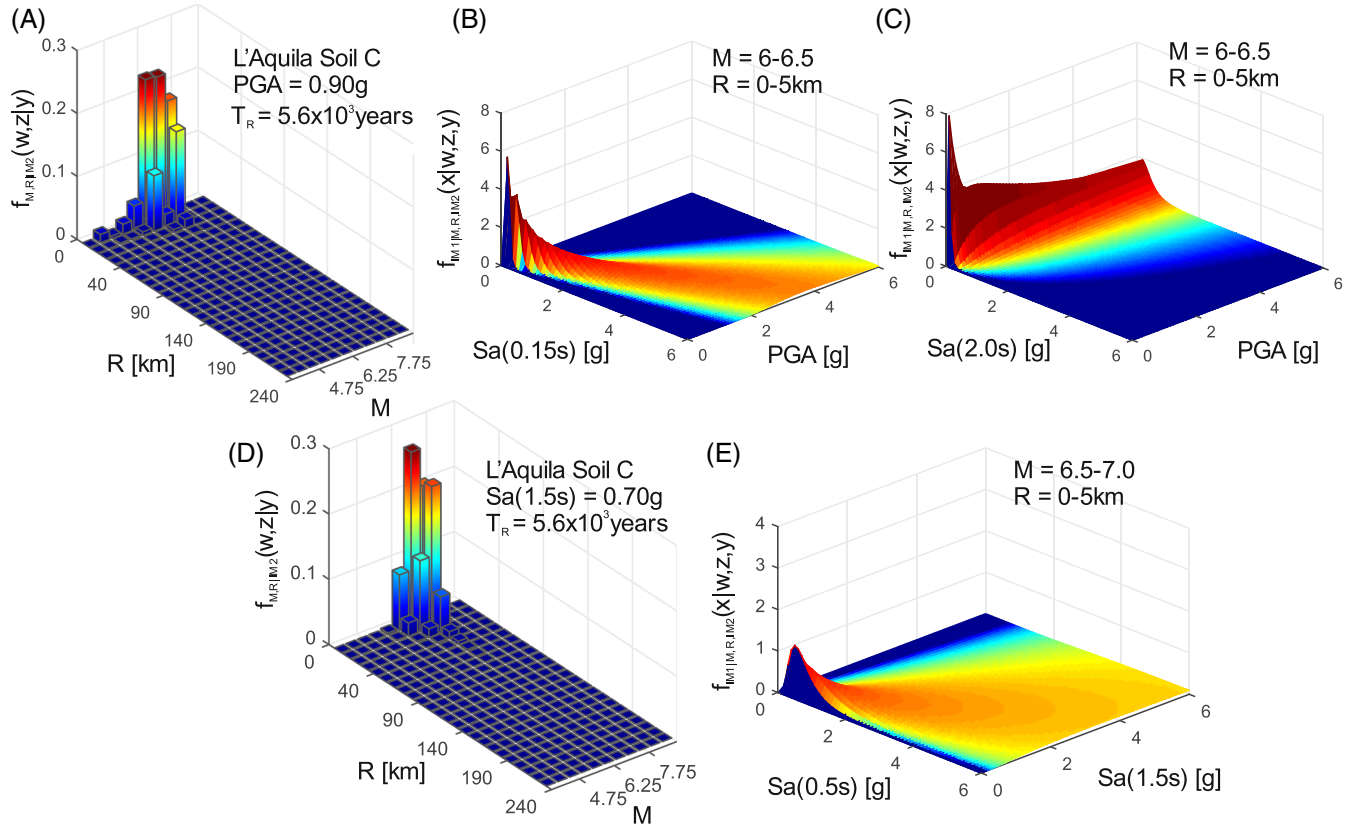

FIGURE 3 Probabilistic seismic hazard analysis (PSHA) results; (A) hazard disaggregation for peak ground acceleration (PGA) = 0.90 g corresponding to $T_R = 5.6 \times 10^3$ year at L'Aquila; examples of conditional probability density function (PDF) of (B) *Sa*(0.15 s) and (C) *Sa*(2.0 s) given PGA; (D) hazard disaggregation for *Sa*(1.5 s) = 0.70 g corresponding to $T_R = 5.6 \times 10^3$ year at L'Aquila; example of conditional PDF of (E) *Sa*(0.5 s) given *Sa*(1.5 s)

5.4 | Reference fragility analysis

As illustrated in Figure 4A,B, the reference fragility assessment involved MSA performed in a similar manner to the original fragility assessment (Figure 2A,B), yet considering seismic input based on site's hazard in terms of IM_2. Since record sets selected based on the PGA hazard were not available from the datasets of the RINTC project, ad-hoc GM

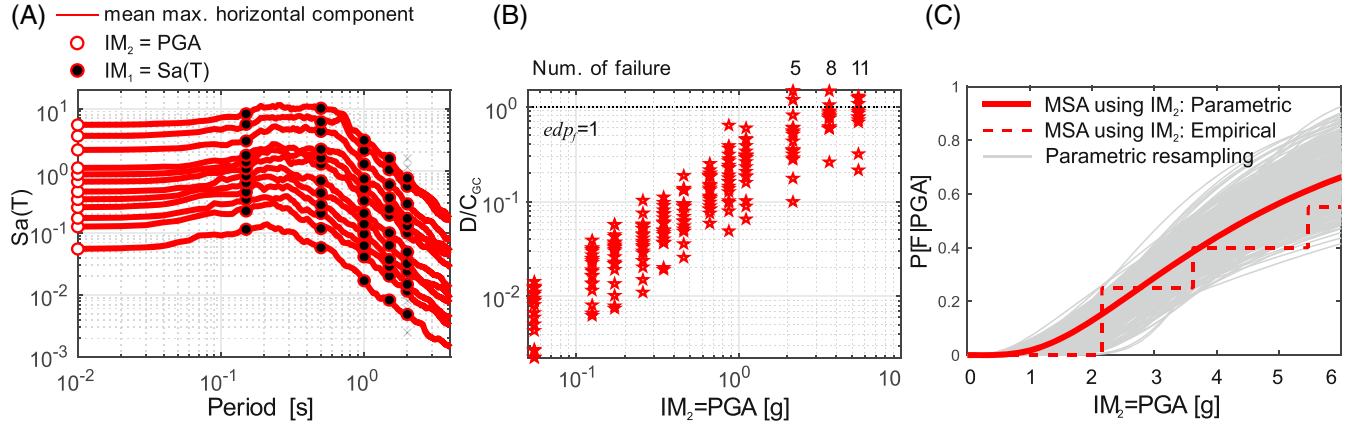

FIGURE 4 MSA for reference target fragility: (A) mean spectra of ground motion (GM) records, (B) collapse demand-over-capacity (*D/C*) ratios and number of failure cases, and (C) reference target fragility estimated via maximum likelihood

record sets were selected for the multiple PGA values (ie, stripes). The target CS given a certain PGA value was computed via the hazard models used in PSHA, then 20 GM records were selected from the NESS database[52] so as to match the target CS pertaining to each stripe (Figure 4A).

It should be noted that the PGA domain was discretized through the exceedance return periods specified above, plus two additional return periods corresponding to $T_R = 10^6$ and $T_R = 10^7$ years (ie, 12 stripes in total). The additional two PGA levels were considered so as to render the reference fragility up to a large PGA level. In fact, generally, a small number of the GC cases was observed even at the tenth PGA value (eg, five failure cases, as shown in Figure 4B), thus the analysis was continued, in the majority of the cases, until the number of GC failure cases had reached more than 50% of the total number of the records per stripe (ie, more than 10). As it regards the cases when the target IM is *Sa* at $T = \{1.0\text{s}, 1.5\text{s}, 2.0\text{ s}\}$, the GM record sets collected in the RINTC project (ie, those used above for the original fragility assessment of the BF and/or 9st buildings) were used.

Whereas the original fragility assessment (in Sections 5.1 and 5.2) employed only the parametric approach, the reference fragility functions were evaluated by both (a) nonparametric and (b) parametric approaches (Figure 4C). The former was adopted to interpret as-observed probability distributions without involving any particular assumptions on the probabilistic model. The latter was used to make the converted and reference curves comparable by means of a few parameters, including uncertainty of estimation. For each, $i - th$ stripe of $IM_2 = y_i$, nonparametric fragility was given by Equation (11) counting the number of the observations of structural failure, $N_{f,IM_2=y_i}$ out of the total number of records at each stripe, $N_{tot,IM_2=y_i}$:

$$P[F|IM_2 = y_i] = \frac{N_{f,IM_2=y_i}}{N_{tot,IM_2=y_i}}. \tag{11}$$

In the parametric approach, a lognormal cumulative distribution function in Equation (12) was assumed as follows:

$$P[F|IM_2 = y] = \Phi\left(\frac{\ln y - \ln\hat{\theta}}{\hat{\beta}}\right). \tag{12}$$

The $\{\hat{\theta},\hat{\beta}\}$ parameters in the equation were estimated through a maximum likelihood estimation criterion[53] based on the EDP vectors observed at multiple (m) IM_2 stripes, $edp_i = \left\{edp_1, edp_2, ..., edp_{N_{tot},IM_2=y_i}\right\}$, $i = \{1,2,...,m\}$, which are partitioned into $N_{f,IM_2=y_i}$ failure cases and $\left(N_{tot,IM_2=y_i} - N_{f,IM_2=y_i}\right)$ nonfailure cases as follows:

$$\{\hat{\theta},\hat{\beta}\} = \underset{\theta,\beta}{\operatorname{argmax}}\left[\sum_{i=1}^{m} \ln\binom{N_{tot,IM_2=y_i}}{N_{f,IM_2=y_i}} + N_{f,IM_2=y_i}\ln\left\{\Phi\left[\frac{\ln(y_i/\theta)}{\beta}\right]\right\} + \left(N_{tot,IM_2=y_i} - N_{f,IM_2=y_i}\right)\cdot\ln\left\{1-\Phi\left[\frac{\ln(y_i/\theta)}{\beta}\right]\right\}\right]. \tag{13}$$

It should be mentioned that one can also estimate the reference fragility through the regression-based approach which was adopted in the original fragility assessment. This study selected the EDP-based maximum likelihood estimation approach, which is convenient when structural response is evaluated, using a scalar IM, by means of MSA.

Table 6 shows the results of the estimated fragility parameters with respect to PGA for the nine structures, and Table 7 provides those with respect to spectral acceleration at the three periods examined for the 6st IF building. To assess the estimation uncertainties, the expected value and standard deviation of each fragility parameter were estimated through parametric resampling.[32] In each table, the expected value ($E[\bullet]$) and coefficient of variation (CoV) of $\{\hat{\theta},\hat{\beta}\}$ are provided. It can be seen that the low-rise structures with relatively small fundamental vibration periods tend to show a smaller expected value of median PGA causing failure, $E\left[\hat{\theta}_{PGA}\right]$, compared with the taller buildings featuring relatively large vibration periods. This trend is clearly seen in $\hat{\theta}_{PGA}$, particularly with respect to GC. The logarithmic standard deviation also shows the increasing trends of the mean and variance with the vibration period of the structure and with the performance level: $E\left[\hat{\beta}_{PGA}\right]$ varies between 0.37 and 0.52 for the UPD and 0.49 and 0.89 for the GC fragilities, being associated with the CoVs of 13% to 15% and 19% to 30%, respectively.

TABLE 6 Estimated lognormal fragility parameters in reference analyses (IM_2≡PGA)

	PL	UPD						GC					
	Config.	BF		IF		PF		BF		IF		PF	
Story	Parameter	$E[\bullet]$	CoV	$E[\bullet]$	CoV	$E[\bullet]$	CoV	$E[\bullet]$	CoV	$E[\bullet]$	CoV	$E[\bullet]$	CoV
3st	$\hat{\theta}_{PGA}$, g	0.29	7%	0.32	5%	0.45	6%	3.90	11%	3.34	9%	3.91	11%
	$\hat{\beta}_{PGA}$	0.51	13%	0.37	15%	0.43	14%	0.62	20%	0.49	19%	0.55	19%
6st	$\hat{\theta}_{PGA}$, g	0.44	6%	0.62	6%	0.56	6%	5.32	20%	4.67	15%	4.54	14%
	$\hat{\beta}_{PGA}$	0.41	14%	0.41	14%	0.40	14%	0.74	25%	0.69	21%	0.69	22%
9st	$\hat{\theta}_{PGA}$, g	0.54	7%	0.50	5%	0.47	7%	8.37	39%	7.41	33%	7.37	34%
	$\hat{\beta}_{PGA}$	0.48	13%	0.38	14%	0.52	13%	0.89	30%	0.75	30%	0.81	29%

Abbreviations: BF, bare-frame; CoV, coefficient of variation; GC, global collapse; IF, infilled-frame; IM, intensity measure; PF, *pilotis*-frame; PGA, peak ground acceleration; PL, performance level; UPD, usability-preventing damage; 3st, three-story; 6st, six-story; 9st, nine-story.

TABLE 7 Estimated lognormal fragility parameters in reference analyses ($IM_2 \equiv Sa(T > 0.5\ s)$)

	PL	UPD						GC					
Config.	IM_2	Sa(1.0 s)		Sa(1.5 s)		Sa(2.0 s)		Sa(1.0 s)		Sa(1.5 s)		Sa(2.0 s)	
6st IF	Parameter	$E[\bullet]$	CoV	$E[\bullet]$	CoV	$E[\bullet]$	CoV	$E[\bullet]$	CoV	$E[\bullet]$	CoV	$E[\bullet]$	CoV
	$\hat{\theta}_{Sa(T)}$, g	0.58	6%	0.29	9%	0.19	9%	3.42	10%	1.88	9%	1.85	70%
	$\hat{\beta}_{Sa(T)}$	0.30	20%	0.61	14%	0.59	14%	0.27	61%	0.25	55%	0.46	78%

Abbreviations: CoV, coefficient of variation; GC, global collapse; IF, infilled-frame; IM, intensity measure; PL, performance level; UPD, usability-preventing damage; 6st, six-story.

Table 7 shows the lognormal fragility parameters of the same 6st IF building, yet expressed in terms of $Sa(T)$ at the three different periods, $T = \{1.0\text{s}, 1.5\text{s}, 2.0\text{s}\}$, ie, $\left\{\hat{\theta}_{Sa(T)}, \hat{\beta}_{Sa(T)}\right\}$. $E\left[\hat{\theta}_{Sa(T)}\right]$ decreases with an increase of the vibration period of the target IM, while $E\left[\hat{\beta}_{Sa(T)}\right]$ increases with it. For both of the two parameters, larger CoVs were observed particularly with respect to the GC performance, as expected. The plots of the reference fragility curves, obtained via nonparametric, parametric, and parametric resampling approaches, are all provided in the following section in comparison with the IM conversion results. As an example, the resampled fragility curves, corresponding to 500 simulations are given as gray lines in Figure 4C.

6 | RESULTS AND DISCUSSION

6.1 | IM conversion to PGA

This subsection presents the results of the IM conversion from $Sa(T)$ to PGA for both the UPD and GC fragility curves. For each of the nine buildings, the three conversion cases were compared with the results from the reference analyses.

6.1.1 | Usability-preventing damage

The PGA-based fragility curves were derived from the original fragility functions and site-specific hazard functions through the conversion formulas of Equations (2) to (4). The results of the three conversion cases, involving $\{IM_1, IM_2, M, R\}$, $\{IM_1, IM_2\}$, and IM_1, are presented in Figure 5 for the nine building cases, together with the reference analysis results. It can be observed that all three conversion cases show apparently comparable results in the cases where the scalar IM_1 has a comparable explicative power with respect to the vector-valued IMs.

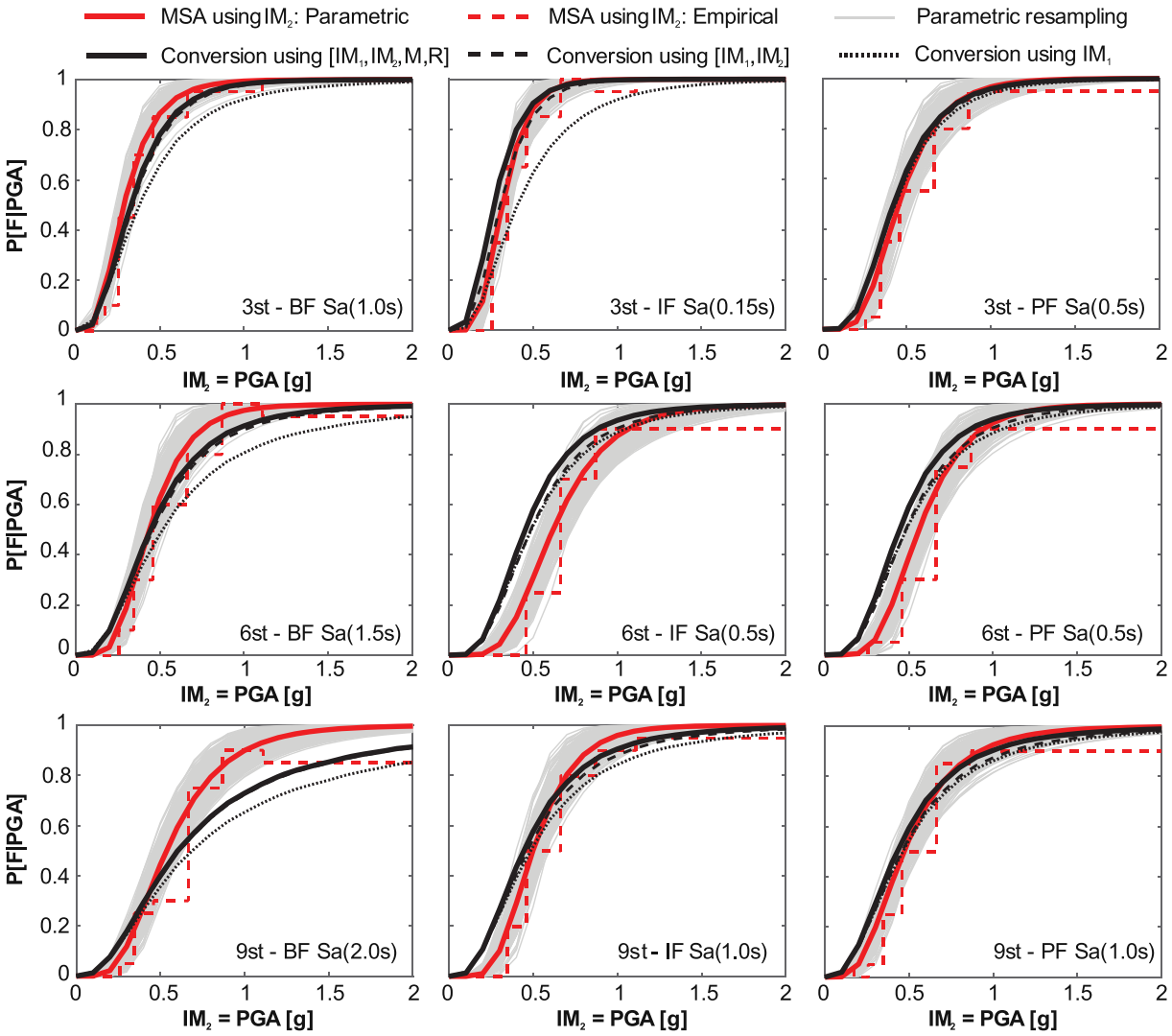

FIGURE 5 Comparison of converted and reference fragility curves with respect to usability-preventing damage (UPD) ($IM_2 \equiv$PGA)

Conversely, it can be seen that the curves converted using the vector-valued IMs have better agreement with the reference curves (empirical and parametric) at upper tails in the cases where the two-parameter vector $\{IM_1, IM_2\}$ has a singificanly larger explicative power than IM_1 alone (3st and 6st BF). As it regards the reference fragilities, the lognormal fragility fits the empirical one, except the largest period structure (9st BF) where some discrepancies appear at larger PGA values. In this case, the converted fragility curves apparently track better the empirical one than the set of parametric fragility curves, which are constrained to a fixed shape.

It can be also seen that most of the conversion cases rendered the fragility estimates within the band of the resampled fragility curves indicating estimation uncertainties. Particularly, the conversion involving the optimal IM led to the median estimates $\left(\hat{\theta}_{PGA}\right)$ with 1% to 29% difference from the expected values from the parametric resampling.

6.1.2 | Global collapse

The results of the collapse fragility curves in terms of PGA are presented in Figure 6 for the nine building cases. The results not only show somewhat similar trends as the UPD fragilities, but also may support that the performance of the IM conversion depends on the combination of the original and target IMs.[#]

[#]Also, it should be noted that the local non-monotonicity of the converted fragilities at larger intensity measure (IM) levels are a numerical issue, mainly deriving from the way disaggregation results are discretized in the applications.

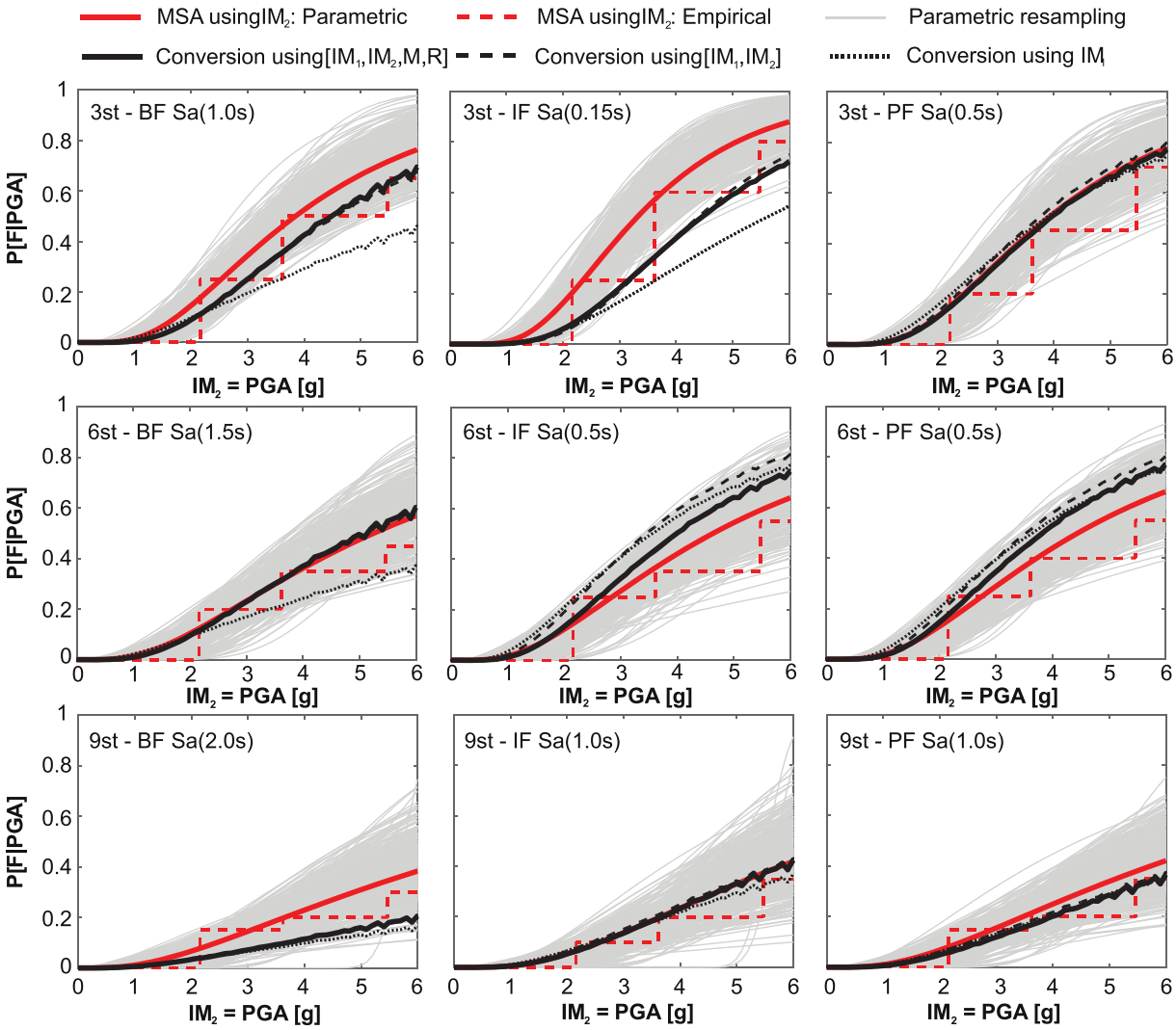

FIGURE 6 Comparison of converted and reference fragility curves with respect to global collapse (GC) ($IM_2 \equiv$PGA)

In cases of converting from an intermediate period ranging from 0.5 to 1.5 seconds, the conversion approaches provided apparently comparable results to the reference curves in most of the cases. Indeed, the median estimates $\left(\hat{\theta}_{PGA}\right)$ feature 1% to 23% differences with respect to the expected value estimated from the resampled parametric fragilities, $E\left[\hat{\theta}_{PGA}\right]$. On the contrary, larger discrepancies with the target fragility estimates were observed in the IM conversions from the spectral acceleration at the smallest and the largest periods (ie, 3st IF and 9st BF where IM_1 is Sa(0.15s) and Sa(2.0s), respectively). With respect to the former, all converted fragility curves were located at the right side of the reference fragility functions, presumably because of regression involving relatively more correlated IMs ($\rho_{\ln IM_1, \ln IM_2} \cong 0.89$), which also seem to have affected somewhat the estimates of the UPD fragility curves. Regarding the conversion from Sa(2.0 s), larger discrepancies are associated with the validity domain of the regression model. As shown in Figure 3C, the major PDF contribution comes from a quite limited range of the $IM_1 - IM_2$ domain (ie, corresponding to low values of IM_1). In fact, the structural response data at large IM_2 levels were rarely obtained under the seismic input conditional on IM_1 due to a relatively low correlation between the two IMs ($\rho_{\ln IM_1, \ln IM_2} \cong 0.35$). In such a case, the choice of regression models and/or fragility assessment procedures is also an issue. The resulting converted fragility can be sensitive to the form of the fragility surface in the local area with dominant hazard contribution.

Figure 7 illustrates the abovementioned issues showing the fragility surfaces in the $Sa(T) - PGA$ domain with respect to the considered two PLs. In each panel of the figure, the data points used for the regression analyses are plotted together with the iso-probability lines for the fragility surfaces (for the sake of illustration, the plotted models

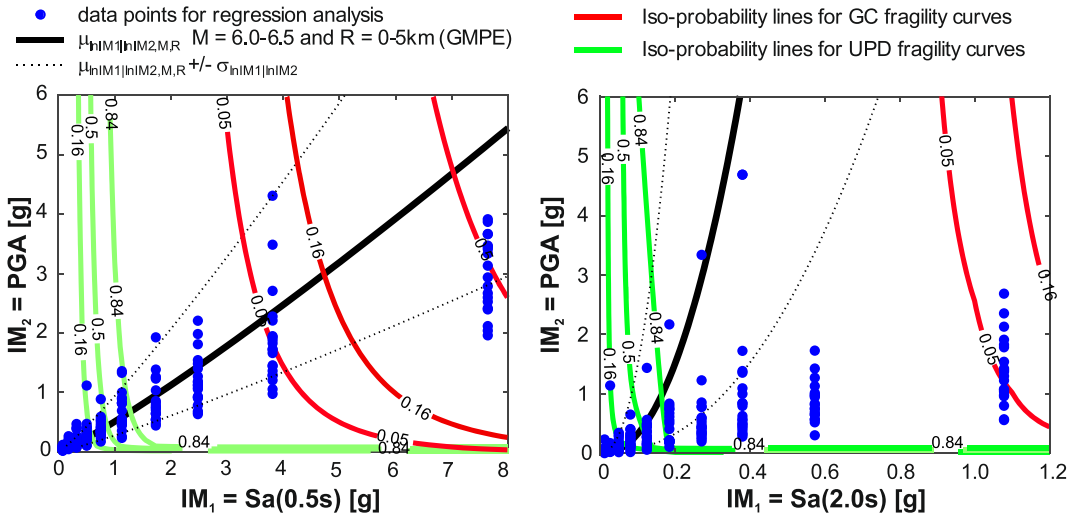

FIGURE 7 Comparisons of the fragility surfaces with respect to the two performance levels and the ground motion prediction equation (GMPE) models: (left) six-story (6st) infilled-frame (IF) and (right) nine-story (9st) bare-frame (BF)

correspond to the surfaces computed using $\{IM_1, IM_2\}$). The figure also provides $\mu_{\ln IM_1|\ln IM_2,M,R}$ and $\sigma_{\ln IM_1|\ln IM_2}$ from Equation (6), given a certain earthquake scenario, namely, the lognormal parameters of the conditional PDF of IM_1, $f_{IM_1|M,R,IM_2}$, given IM_2 and the $M - R$ scenario dominating the hazard disaggregation in Figure 3A. The left panel corresponds to the conversion from Sa(0.5 s) to PGA ($\rho_{\ln IM_1,\ln IM_2} \cong 0.69$), while the right one shows the probabilistic models for the conversion from Sa(2.0 s). It can be clearly observed that, when the two IMs are moderately correlated (corresponding to the former), the data points defining the fragility surfaces (scatters in the figure) cover the range corresponding to a high value of the conditional distribution function of IM_1 given IM_2 (dashed and solid black lines). Thus, the conversion integral beyond the domain of the datapoints does not significantly matter as its effect is compensated by the integration with the seismic hazard, which is low in this domain. Conversely, many of the data points in the right panel lie beyond the $IM_1 - IM_2$ range corresponding to a large value of the conditional PDF, thus this kind of *model extrapolation* can substantially affect the converted fragility, in particular, with respect to the GC. Furthermore, in this conversion case, the underestimation of the probability that the structure fails according to the GC criterion (ie, the 9st BF building in Figure 6) can be also ascribed to the small probabilities deriving from the fitted linear regression model in the $IM_1 - IM_2$ domain where the hazard term is significant.

6.2 | IM conversion to spectral acceleration at a larger period

The IM conversions from Sa(0.5 s) to $Sa(T > 0.5$ s) were also performed in a similar manner. The results of the IM conversions with respect to the two PLs are shown in Figure 8 for all three cases. Regarding the fragilities with respect to UPD, all converted fragility curves derived from the linear regression models are generally in agreement with the reference curves, although the curves in terms of Sa(1.0 s) are located slightly at the left side to the group of the reference fragilities. When the GC fragility is concerned, however, all log-linear regression-driven fragility curves (denoted LR in the figure) resulted to underestimate the reference fragility at large IM_2 levels (eg, beyond the ninth stripe where Sa(1.5 s) = 1.0 g, corresponding to $T_R = 10^4$ years). In such cases, the hybrid models utilizing the logistic regression apparently capture better the target curves from the reference MSA up to the largest IM_2 level (corresponding to $T_R = 10^5$ years; eg, Sa(1.5 s) = 2.0 g). Although large discrepancies at extremely large IM levels generally may not significantly matter when integrated with a hazard curve to obtain the failure rate, the shape of the resulting GC fragility depends on the functional form adopted in the original fragility assessment. It should also be noted that the GC fragility conversion to Sa(2.0 s), again, turned out to be an exception due to the extension of the regression model far beyond the observation range (see the previous subsection).

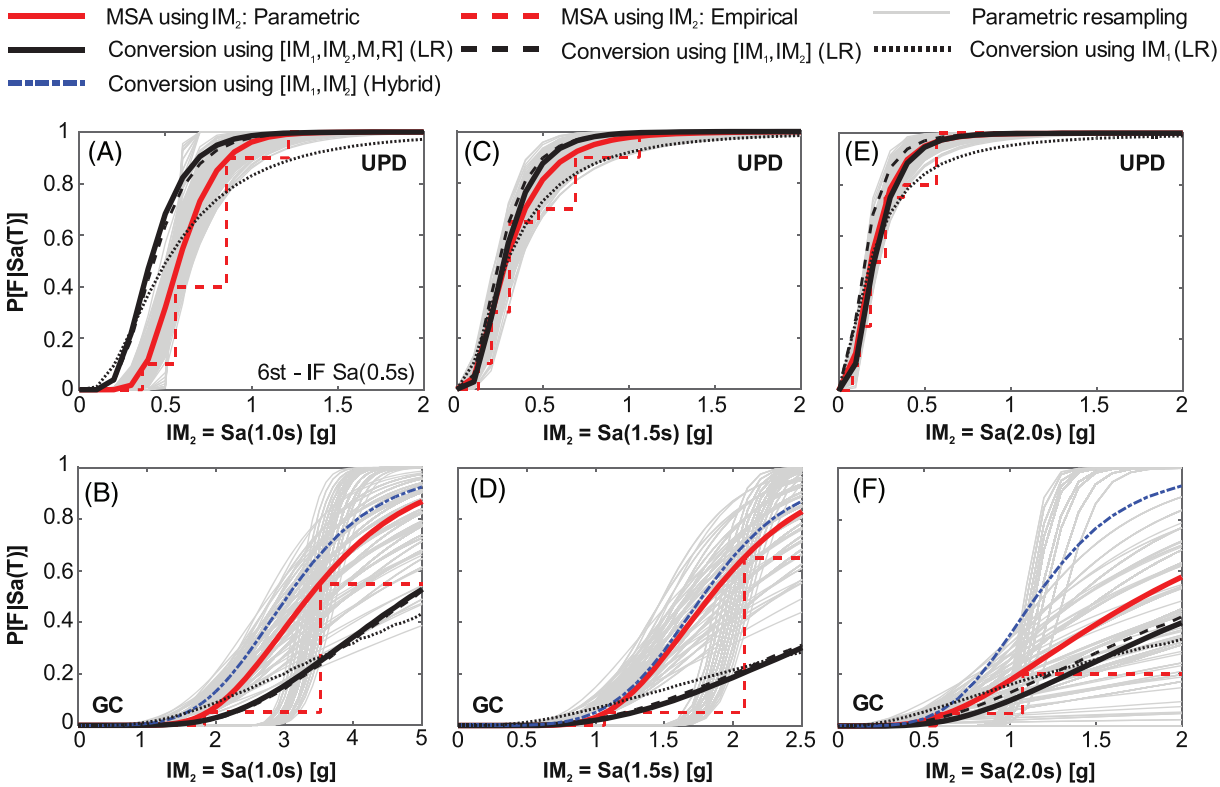

FIGURE 8 Comparison of converted and reference fragility curves in cases of $IM_2 \equiv Sa(T > 0.5\text{ s})$: (A,B) to $Sa(1.0\text{ s})$, (C,D) to $Sa(1.5\text{ s})$, and (E,F) to $Sa(2.0\text{ s})$

7 | CONCLUSIONS

The study discussed the probabilistic framework for converting spectral acceleration-based IMs of fragility curves with the aid of the state-of-the-art methods within PBEE. On the premise that structural response given an IM is available from a preliminary structural response analysis, the framework aims to express the fragility curve in terms of a target IM without any additional structural analyses.

The IM conversion cases were explored using the ESDoF systems of multi-story Italian code-conforming RC buildings featuring a wide range of the fundamental vibration period of the structure (from 0.3-2.0 seconds). For each structure, the original IM was defined as spectral acceleration at a period close to the fundamental period of the structure, $Sa(T)$. Then, the IM conversions were performed with respect to two performance levels (ie, UPD and GC) and under two different conditions: (a) the target IM is the spectral acceleration at a period smaller than that of the original IM (ie, PGA) for all considered structures and (b) the target IM is the spectral acceleration at a period larger than that of the original IM for a structure, that is, 0.5 seconds. For all IM conversion cases, the fragility curves, expressed in terms of the target IM, were obtained from the regressions of the structural response given $Sa(T)$ on the involved IM variables and functions computed from the PSHA for the building site. The converted fragility functions were compared with the results of the reference fragility analysis, also accounting for the estimation uncertainties. Notable remarks are summarized in the following:

1. Owing to the use of mostly sufficient IMs and the hazard-consistent record selection for structural response assessment, the effects of magnitude and source-to-site distance did not affect significantly the resulting converted fragility functions. Nevertheless, it was also observed that the use of a two-parameter vector IM consisting of the original and target IMs exhibited better agreement with the reference fragility curves in some cases.
2. It was observed that the choice of fragility modelling approaches affected the resulting fragilities, possibly depending on the correlation and/or the interaction between the original and target IMs. In cases of converting to spectral acceleration at a period smaller than that of the original IM (ie, to PGA), the linear regression models were used to model the original fragility functions. Mostly, the converted PGA fragility curves resulted to be within the range of

reference curves, ie, parametric fragility functions including estimation uncertainties. The larger discrepancies with the reference analysis results were observed in the conversions from spectral acceleration at the smallest or the largest period among those considered. The former can be due to the used regression model to link structural response with variables including two spectral accelerations at close periods, while the latter can be related to the use of the fragility model beyond the domain where response data belong. These trends were clearer particularly when referring to the attainment of GC.

3. In cases of converting to spectral acceleration at a larger period than that of the original IM, the results suggested that it is necessary to carefully investigate a fragility model. The results from multiple linear regression models showed consistency with the reference curves (both empirical and parametric) for UPD. Conversely, the hybrid models, combining the linear and logistic regressions, showed better agreement for the GC performance levels.

The procedures described in the paper can be of help to the structural engineers dealing with fragility functions in terms of different IMs. Besides other meaningful metrics, such as the structural failure rate, this allows an informative comparison of structural vulnerability.

ACKNOWLEDGEMENTS

The study presented in this article was developed within the activities of the ReLUIS-DPC 2014-2018 research program, funded by Presidenza del Consiglio dei Ministri – Dipartimento della Protezione *Civile (DPC)* and the European Comission, Horizon 2020 program grant number 691213 entitled "Experimental Computational Hybrid Assessment of Natural Gas Pipelines Exposed to Seismic Risk" (*EXCHANGE-RISK*). The comments on early drafts from Georgios Baltzopoulos (Università degli Studi di Napoli Federico II, Italy) and Eugenio Chioccarelli (Università Telematica Pegaso, Italy) are also gratefully acknowledged. Furthermore, the authors are grateful to the two anonymous reviewers who helped to improve the quality of the paper.

ORCID

Akiko Suzuki https://orcid.org/0000-0001-9523-3488
Iunio Iervolino https://orcid.org/0000-0002-4076-2718

REFERENCES

1. Luco N. Probabilistic seismic demand analysis, SMRF connection fracutures, and near-source effects. Ph. D. Thesis, Department of Civil and Environmental Engineering, Stanford Unviersity, CA, USA [Advisor: C. A. Cornell], 2002.
2. Tothong P, Luco N. Probabilistic seismic demand analysis using advanced ground motion intensity measures. *Earthq Eng Struct Dyn.* 2007;36(13):1837-1860. https://doi.org/10.1002/eqe.696
3. Giovenale P, Cornell CA, Esteva L. Comparing the adequacy of alternative ground motion intensity measures for the estimation of structural responses. *Earthq Eng Struct Dyn.* 2004;33(8):951-979. https://doi.org/10.1002/eqe.386
4. Shome N, Cornell CA. Structural seismic demand analysis: consideration of "collapse.". In: *Proceedings of 8th ACSE Specialty Conference on Probabilistic Mechanics and Structural Reliability*. South Bend, Indiana, USA; 2000.
5. Shome N. Probabilistic seismic demand analysis of nonlinear structures. Ph. D. Thesis, Department of Civil and Environmental Engineering, Stanford Unviersity, CA, USA [Advisor: C. A. Cornell], 1999.
6. Baker JW, Cornell CA. A vector-valued ground motion intensity measure consisting of spectral acceleration and epsilon. *Earthq Eng Struct Dyn.* 2005;34(10):1193-1217. https://doi.org/10.1002/eqe.474
7. Baker JW. Probabilistic structural response assessment using vector-valued intensity measures. *Earthq Eng Struct Dyn.* 2007;36(13):1861-1883. https://doi.org/10.1002/eqe.700
8. Vamvatsikos D, Cornell CA. Developing efficient scalar and vector intensity measures for IDA capacity estimation by incorporating elastic spectral shape information. *Earthq Eng Struct Dyn.* 2005;34(13):1573-1600. https://doi.org/10.1002/eqe.496
9. Bojórquez E, Iervolino I. Spectral shape proxies and nonlinear structural response. *Soil Dyn Earthq Eng.* 2011;31(7):996-1008. https://doi.org/10.1016/j.soildyn.2011.03.006
10. Eads L, Miranda E, Lignos DG. Average spectral acceleration as an intensity measure for collapse risk assessment. *Earthq Eng Struct Dyn.* 2015;44(12):2057-2073. https://doi.org/10.1002/eqe.2575
11. Giardini D, Grünthal G, Shedlock KM, Zhang P. The GSHAP global seismic hazard map. *Ann Geophys.* 1999;42(6):1225-1230. https://doi.org/10.4401/ag-3784
12. Stafford PJ. Evaluation of structural performance in the immediate aftermath of an earthquake: a case study of the 2011 Christchurch earthquake. *Int J Forensic Eng.* 2012;1(1):58-77. https://doi.org/10.1504/IJFE.2012.047447
13. Weatherill GA, Silva V, Crowley H, Bazzurro P. Exploring the impact of spatial correlations and uncertainties for portfolio analysis in probabilistic seismic loss estimation. *Bull Earthq Eng.* 2015;13(4):957-981. https://doi.org/10.1007/s10518-015-9730-5

14. Michel C, Crowley H, Hannewald P, Lestuzzi P, Fäh D. Deriving fragility functions from bilinearized capacity curves for earthquake scenario modelling using the conditional spectrum. *Bull Earthq Eng.* 2018;16(10):4639-4660. https://doi.org/10.1007/s10518-018-0371-3
15. Iervolino I, Spillatura A, Bazzurro P. Seismic reliability of code-conforming Italian buildings. *J Earthq Eng*. 2018;22(sup2):5-27. https://doi.org/10.1080/13632469.2018.1540372
16. Suzuki A, Iervolino I. Seismic fragility of code-conforming Italian buildings based on SDoF approximation. *J Earthq Eng.* 2019;1-35. https://doi.org/10.1080/13632469.2019.1657989
17. Kennedy RP. Overview of methods for seismic PRA and margin analysis including recent innovations. In: *The OECD-NEA Workshop on Seismic Risk*. Tokyo: Japan; 1999:10-12.
18. Huang Y-N, Whittaker AS, Luco N. A probabilistic seismic risk assessment procedure for nuclear power plants: (I) Methodology. *Nucl Eng Des.* 2011;241(9):3996-4003. https://doi.org/10.1016/J.NUCENGDES.2011.06.051
19. Ohtori Y, Hirata K. *Conversion Methods of Ground Motion Index for Fragility Curve, CRIEPI Civil Engineering Research Laboratory Rep. No.N05053* (in Japanese). Tokyo, Japan; 2007.
20. Melchers RE, Beck AT. *Structural Reliability Analysis and Prediction*. John Wiley & Sons, Ltd.
21. Suzuki A, Iervolino I. Hazard-consistent intensity measure conversion of fragility curves. In: *13th International Conference on Applications of Statistics and Probability in Civil Engineering*. Seoul, South Korea; 2019.
22. Cornell CA, Krawinkler H. *Progress and Challenges in Seismic Performance Assessment, PEER Center News, 3, 1-3*. CA, USA; 2000.
23. Jalayer F. Direct probabilistic seismic analysis: implementing non-linear dynamic assessments. Ph. D. Thesis, Department of Civil and Environmental Engineering, Stanford Unviersity, CA, USA [Advisor: C. A. Cornell], 2003.
24. Lin T, Haselton CB, Baker JW. Conditional spectrum-based ground motion selection. Part I: hazard consistency for risk-based assessments. *Earthq Eng Struct Dyn.* 2013;42(12):1847-1865. https://doi.org/10.1002/eqe.2301
25. Cornell CA. Engineering seismic risk analysis. *Bull Seismol Soc Am.* 1968;58(5):1583-1606.
26. Iervolino I, Giorgio M, Galasso C, Manfredi G. Conditional hazard maps for secondary intensity measures. *Bull Seismol Soc Am.* 2010;100(6):3312-3319. https://doi.org/10.1785/0120090383
27. Bazzurro P, Cornell CA. Vector-valued probabilistic seismic hazard analysis. In: *7th U.S. National Conference on Earthquake Engineering*. Vol.10; 2002.
28. Bazzurro P, Cornell CA. Disaggregation of seismic hazard. *Bull Seismol Soc Am.* 1999;89(2):501-520. https://doi.org/10.1785/0120060093
29. Baker JW, Jayaram N. Correlation of spectral acceleration values from NGA ground motion models. *Earthq Spectra.* 2008;24(1):299-317. https://doi.org/10.1193/1.2857544
30. Cornell CA, Jalayer F, Hamburger RO, Foutch DA. Probabilistic basis for 2000 SAC federal emergency management agency steel moment frame guidelines. *J Struct Eng.* 2002;128(4):526-533. https://doi.org/10.1061/ASCE0733-94452002128:4526
31. Vamvatsikos D, Cornell CA. Incremental dynamic analysis. *Earthq Eng Struct Dyn.* 2002;31(3):491-514. https://doi.org/10.1002/eqe.141
32. Iervolino I. Assessing uncertainty in estimation of seismic response for PBEE. *Earthq Eng Struct Dyn.* 2017;46(10):1711-1723. https://doi.org/10.1002/eqe.2883
33. Elefante L, Jalayer F, Iervolino I, Manfredi G. Disaggregation-based response weighting scheme for seismic risk assessment of structures. *Soil Dyn Earthq Eng.* 2010;30(12):1513-1527. https://doi.org/10.1016/j.soildyn.2010.07.003
34. CS.LL.PP. Norme tecniche per le costruzioni (in Italian). 2008.
35. CS.LL.PP. Aggiornamento delle norme tecniche per le costruzioni (In Italian). 2018.
36. Ricci P, Manfredi V, Noto F, et al. Modeling and seismic response analysis of italian code-conforming reinforced concrete buildings. *J Earthq Eng.* 2018;22(sup2):105-139. https://doi.org/10.1080/13632469.2018.1527733
37. CEN. Eurocode 8: Design Provisions for Earthquake Resistance of Structures, Part 1.1: General rules, seismic actions and rules for buildings, EN1998-1. 2004.
38. McGuire RK. Probabilistic seismic hazard analysis and design earthquakes: closing the loop. *Bull Seismol Soc Am.* 1995;85(5):1275-1284.
39. McKenna F, Fenves GL, Scott MH, Jeremic B. Open System for Earthquake Engineering Simulation (OpenSees). http://opensees.berkeley.edu/. Published 2000. .
40. Fajfar P. A nonlinear analysis method for performance-based seismic design. *Earthq Spectra.* 2000;16(3):573-592. https://doi.org/10.1193/1.1586128
41. Baltzopoulos G, Baraschino R, Iervolino I, Vamvatsikos D. SPO2FRAG: software for seismic fragility assessment based on static pushover. *Bull Earthq Eng.* 2017;15(10):4399-4425. https://doi.org/10.1007/s10518-017-0145-3
42. Vamvatsikos D, Cornell CA. Direct estimation of the seismic demand and capacity of oscillators with multi-linear static pushovers through IDA. *Earthq Eng Struct Dyn.* 2006;35(9):1097-1117. https://doi.org/10.1002/eqe.573
43. Suzuki A, Baltzopoulos G, Iervolino I. RINTC-Workgroup. A look at the seismic risk of Italian code-conforming RC buildings. In: *Proceedings of 16th European Conference on Earthquake Engineering*. Thessaloniki, Greece; 2018:18-21.
44. Suzuki A. Seismic fragility assessment of code-conforming buildings in Italy. Ph. D. Thesis, Dipartimento di Strutture per l'Ingegneria e l'Architettura, Università degli Studi di Napoli Federico II, Naples, Italy [Advisor: I. Iervolino], 2019.
45. Kohrangi M, Bazzurro P, Vamvatsikos D, Spillatura A. Conditional spectrum-based ground motion record selection using average spectral acceleration. *Earthq Eng Struct Dyn.* 2017;46(10):1667-1685. https://doi.org/10.1002/eqe.2876
46. Luco N, Cornell CA. Structure-specific scalar intensity measures for near-source and ordinary earthquake ground motions. *Earthq Spectra.* 2007;23(2):357-392. https://doi.org/10.1193/1.2723158

47. Padgett JE, Nielson BG, DesRoches R. Selection of optimal intensity measures in probabilistic seismic demand models of highway bridge portfolios. *Earthq Eng Struct Dyn.* 2008;37(5):711-725. https://doi.org/10.1002/eqe.782
48. Efron B. Regression and ANOVA with zero-one data: measures of residual variation. *J Am Stat Assoc.* 1978;73(361):113-121. https://doi.org/10.1080/01621459.1978.10480013
49. Ambraseys NN, Simpson KA, Bommer JJ. Prediction of horizontal response spectra in Europe. *Earthq Eng Struct Dyn.* 1996;25(4):371-400. https://doi.org/10.1002/(SICI)1096-9845(199604)25:4<371::AID-EQE550>3.0.CO;2-A
50. Stucchi M, Meletti C, Montaldo V, Crowley H, Calvi GM, Boschi E. Seismic hazard assessment (2003-2009) for the Italian building code. *Bull Seismol Soc Am.* 2011;101(4):1885-1911. https://doi.org/10.1785/0120100130
51. Chioccarelli E, Cito P, Iervolino I, Giorgio M. REASSESS V2.0: software for single- and multi-site probabilistic seismic hazard analysis. *Bull Earthq Eng*. 2018;1-25. https://doi.org/10.1007/s10518-018-00531-x
52. Pacor F, Felicetta C, Lanzano G, et al. NESS1: a worldwide collection of strong-motion data to investigate near-source effects. *Seismol Res Lett.* 2018;89(6):2299-2313. https://doi.org/10.1785/0220180149
53. Baker JW. Efficient analytical fragility function fitting using dynamic structural analysis. *Earthq Spectra.* 2015;31(1):570-599.

How to cite this article: Suzuki A, Iervolino I. Intensity measure conversion of fragility curves. *Earthquake Engng Struct Dyn*. 2020;49:607–629. https://doi.org/10.1002/eqe.3256